Chlorine isotope mantle heterogeneity: Constraints from theoretical first-principles calculations

Xi Liu [a], Hai-Zhen Wei [a,f]*, Yin-Chuan Li [a], A. E. Williams-Jones [b], Jian- Jun Lu [a], Shao-Yong Jiang [c], Ge Dong [a], Jing Ma [d], Christopher J. Eastoe [e]

[a] *State Key Laboratory for Mineral Deposits Research, Department of Earth Sciences and Engineering, Nanjing University, Nanjing 210023, PR China*

[b] *Department of Earth and Planetary Sciences, McGill University, Montreal H3A 0E8, Canada*

[c] *State Key Laboratory of Geological Processes and Mineral Resources, Faculty of Earth Resources, China University of Geosciences, Wuhan 430074, PR China*

[d] *Key Laboratory of Mesoscopic Chemistry of MOE, School of Chemistry & Chemical Engineering, Nanjing University, Nanjing, 210023, PR China*

[e] *Department of Geosciences, University of Arizona, Tucson, Arizona, United States*

[f] *CAS Center for Excellence in Comparative Planetology, China, Anhui 230026, PR China*

* Author to whom correspondence should be addressed:
Prof. Hai-Zhen Wei
School of Earth Sciences and Engineering, Nanjing University
163 Xianlin Avenue, Nanjing, Jiangsu, 210023 PR China
Phone: +86 (25) 89681617; Fax: +86 (25) 89682393
Email address: haizhenwei@nju.edu.cn

ABSTRACT

The processes that caused the heterogeneity of δ^{37}Cl in the Earth's mantle are unclear. Here we report theoretical estimates of equilibrium chlorine isotope fractionation among common chlorine-bearing minerals, namely apatite-group minerals (Cl-Ap, F-Cl-Ap, OH-Cl-Ap), muscovite, phlogopite, tremolite, lizardite, marialite and metal halides, based on first-principles calculations, and use them to provide an explanation for this heterogeneity. Our results show that at ambient P-T conditions, the reduced isotopic partition function ratio (β-factor) is strongly correlated with the metal-Cl bond length/bond strength of the above minerals and that phlogopite and muscovite are more enriched in ^{37}Cl than other minerals. As a result of a number of factors, including the adjacent atomic environment, the sites occupied by chlorine atoms in crystals, the Cl-metal coordination and the crystal density, the sensitivity of $10^3 \ln\beta$ to pressure follows the sequence: halite > fluoro-chlorapatite > chlorapatite > marialite > hydroxyl-chlorapatite > lizardite > tremolite > muscovite > phlogopite. Estimates of the chlorine isotope fractionation between chlorine-bearing minerals and aqueous fluid at the pressure and temperature prevailing during subduction indicate that the δ^{37}Cl values of mantle minerals could vary between -6‰ and +3‰, assuming equilibrium. In contrast, the average δ^{37}Cl value of the bulk mantle is -0.53 ± 0.16‰. Thus, large-scale recycling of volatile Cl from the deep mantle to the continental/oceanic crust and ocean, and the isotopic fractionation of chlorine with increasing metamorphic grade during subduction, could explain the heterogeneity of δ^{37}Cl values observed in mantle materials.

Keywords: Equilibrium chlorine isotope fractionation; chlorine-bearing minerals; P-T-dependent reduced isotopic partition function ratios (β-factor); chlorine isotope mantle heterogeneity

1. Introduction

Chlorine is a volatile and strongly hydrophilic element (Sharp et al., 2010) that has two stable isotopes, ^{35}Cl with 18 neutrons and ^{37}Cl with 20 neutrons. The relative natural abundances of these isotopes are 75.76% and 24.24%, respectively (Berglund and Wieser, 2011). With average concentrations of 30 ppm in the primitive mantle and 244 ppm in the continental crust, chlorine is the most abundant of the halogen group of elements (Palme and O'Neill, 2014; Rudnick and Gao, 2003). It reaches its highest concentration, however, in water. For example, seawater contains 1.9 wt% Cl and the chlorine content of aqueous fluids exsolving from silicate magmas can exceed 10 wt% as a result of the strong preference of chlorine for the aqueous phase (Barnes and Sharp, 2017). This has led to the suggestion that the main hosts of chlorine in the Earth's mantle are fluid inclusions and the OH site in hydrous minerals (e.g., amphibole, mica and apatite) (Luth, 2014).

The various terrestrial chlorine reservoirs have $\delta^{37}Cl$ values that range collectively from -14‰ to +16‰ (Kaufmann et al., 1984; Volpe and Spivack, 1994; Eggenkamp et al., 1995; Willmore et al., 2002; Godon et al., 2004). Most $\delta^{37}Cl$ values are close to 0‰. For example, in evaporites, they vary from -0.5‰ to +0.8‰ (Eastoe et al., 2001; Eggenkamp et al., 2019a, 2019b). Serpentine group minerals have been a particular focus of previous chlorine isotope studies because of the importance of serpentinites in the global chlorine cycle (e.g., Anselmi et al., 2000; Barnes and Sharp, 2006; Bonifacie et al., 2008). The chlorine isotopic composition of serpentinites and related ultramafic rocks has been analyzed for the same reason. Thus, Bonifacie et al. (2008) determined the bulk-rock chlorine content and isotopic composition ($\delta^{37}Cl$) of oceanic serpentinites, high-pressure metaperidotites and associated metasedimentary rocks in order to constrain the contribution of hydrothermal alteration and subduction of oceanic lithosphere to the chlorine content of the mantle and, more broadly, the global chlorine cycle. Much of our information on the chlorine isotopic composition of the mantle comes from the study of mid-ocean ridge basalts (MORBs), which can have relatively wide ranges in $\delta^{37}Cl$ values as shown in Fig. 1. Indeed, Stewart et al. (1998) concluded that enriched mantle reservoirs with a

recycled crustal component are depleted in ^{37}Cl relative to the Standard Mean Oceanic Crust (SMOC), whereas the un-degassed mantle is enriched in ^{37}Cl relative to SMOC. This conclusion is supported by the finding of Bonifacie et al. (2007, 2008) that the mantle source for MORB (degassed) has a $\delta^{37}Cl$ value ≤ -1.6‰. In contrast, analyses of samples representing the subcontinental mantle have yielded $\delta^{37}Cl$ values of 0.01 ± 0.25‰ (Sharp et al., 2007). Contrary to conclusions reached about the chlorine isotopic composition of the mantle based on studies of MORB, those based on Ocean Island Basalts (OIB) record positive values. Thus, John et al. (2010) showed that HIMU-type mantle has $\delta^{37}Cl$ values ranging from -1.6 to +1.1‰, and EM-type mantle values ranging from -0.4 to +2.9‰. Finally, the $\delta^{37}Cl$ values of primary carbonatite, a rock-type representative of small degrees of partially melting of metasomatically altered mantle, vary from -0.8 to +0.1‰; the variation may be greater in some cases due to chlorine isotopic fractionation during post-emplacement evolution of the magma (Eggenkamp and Koster van Groos, 1997). Sharp et al. (2013) measured many additional mantle-derived phases and obtained a tight clustering of $\delta^{37}Cl$ values between -0.3‰ and -0.1‰. The inescapable conclusion of all these studies is that the chlorine isotopic composition of the mantle is extremely heterogeneous (Stewart and Spivack, 2004; Barnes and Sharp, 2017). A question that has not been resolved, however, is the cause(s) of this heterogeneity. One possibility is the subduction of crustal material (e.g., sediment), which some researchers have used to explain the strongly positive $\delta^{37}Cl$ values of EM-type mantle (e.g., John et al., 2010). Another possibility is mantle metasomatism, which Sharp et al. (2007) has used to explain the distinctly lower $\delta^{37}Cl$ values (-1‰) of MORB glasses from the East Pacific Rise.

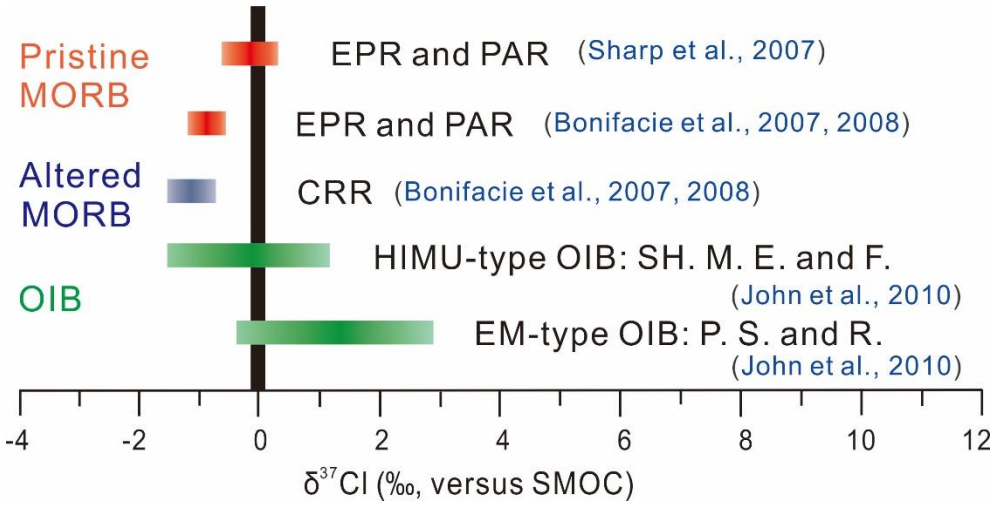

Figure 1. Chlorine isotope variability in mantle-derived materials (Bonifacie et al. 2007, 2008; Sharp et al., 2007; John et al., 2010). EPR: East Pacific Rise; PAR: Pacific Antarctic Ridge; CRR: Costa Rica Rift; SH: St. Helena; M.: McDonald; E.: Easter; F.: Foundation; P.: Pitcairn; S.: Societies; R.: Réunion.

The fractionation of chlorine isotopes by processes such as multiple evaporative cycles (Eggenkamp et al., 1995, 2016, 2019a, 2019b; Eastoe et al., 2001; Eastoe, 2016), diffusion and ion filtration (Eggenkamp et al., 1994; Eggenkamp and Coleman, 2009; Beekman et al., 2011; Agrinier et al., 2019), and water-rock interaction (Barnes and Straub, 2010; Marques et al., 2020) has been well-documented. As a result, chlorine isotopes have found a variety of applications, including tracing the time-dependent processing of volatiles in subduction zones (e.g., Barnes et al., 2008; Barnes and Straub, 2010; Rizzo et al., 2013; Bernal et al., 2014; Chiaradia et al., 2014; Cullen et al., 2015; Li et al., 2015), differentiating fluid types and evaluating evolutionary processes of brine and pore water (e.g., Eggenkamp et al., 1995; Eastoe et al., 1999, 2001; Eastoe, 2016; Shouakar-Stash et al., 2007; Stotler et al., 2010; Alexeeva et al., 2015; Agrinier et al., 2019; Zhao et al., 2021), fingerprinting organic contaminant in hydrologic systems (e.g., Shouakar-Stash et al., 2003, 2006), unraveling chloride sources in soils of the Antarctic dry valleys (e.g., Bao et al., 2008) and constraining the sources of mineralizing fluids in ore deposits (e.g., Eastoe et al., 1989; Eastoe and Guilbert 1992; Bonifacie et al., 2005; Liebscher et al., 2006; Nahnybida et al., 2009; Gleeson and Smith, 2009; Richard et al., 2011; Hanley et al., 2011). The halogen contents and ratios are sensitive monitors for a variety of processes in magmatic-hydrothermal systems, including magmatic fractionation, volatile loss, and fluid-rock interaction (Eggenkamp et al., 2020).

In addition to the above, it is essential to understand the processes responsible for the $\delta^{37}Cl$ heterogeneity of the mantle.

In recent years, considerable progress has been made in theoretically modeling the equilibrium fractionation of stable isotopes among different phases (Schauble, 2004; Schauble et al., 2009; Blanchard et al., 2017). Examples of this include oxygen and silicon isotope fractionation among silicate minerals (Méheut et al., 2007, 2009; Méheut and Schauble, 2014; Huang et al., 2014), oxygen isotope fractionation among hydroxyl-bearing silicates, anhydrous silicate minerals, magnetite, apatite, double carbonates, carbonate and sulfate minerals and between hydroxide minerals and water (Zheng, 1993a, 1993b, 1995, 1996, 1998, 1999; Zheng et al., 1998; Zheng and Böttcher, 2016), magnesium and calcium isotope fractionation among aqueous Mg^{2+}, brucite, silicate, oxide and carbonate minerals (Schauble, 2011, Huang et al., 2013, 2019; Wang et al., 2019; Antonelli et al., 2019) and chlorine isotope fractionation among chlorine-bearing molecules, metal chlorides, silicate minerals, aqueous chloride-gas systems (Schauble et al., 2003; Czarnacki and Halas, 2012; Balan et al., 2019).

The pioneering theoretical study of Schauble et al. (2003) showed that equilibrium chlorine isotopic fractionation is controlled mainly by the oxidation state of Cl and its bonding partner, such that molecules with oxidized Cl concentrate ^{37}Cl relative to chloride, whereas metal chlorides with higher cation electrovalence (e.g., $FeCl_2$, $MnCl_2$) enrich ^{37}Cl relative to those of with lower electrovalence like NaCl, KCl and RbCl (Schauble et al., 2003). This study was the first to estimate the reduced isotopic partition function (β factors) of hydrated Cl^-_{aq}, taking the interaction of the chloride ion with H_2O into account, and the first to calculate chlorine isotopic fractionation factors for Cl_2-HCl-Cl^- aqueous-gas systems (Czarnacki and Halas, 2012). A recent, first-principles, modeling of chlorine isotopic fractionation between Cl-bearing molecules and minerals at ambient pressure clearly documented the importance of the local bonding environment in controlling chlorine isotope fractionation (Balan et al., 2019). As chlorine is one of major volatiles recycled

on a large-scale from the interior to the surface of Earth, measurements of its isotopic composition in earth materials provide a potentially powerful means of tracking the progress of processes like subduction that are important vehicles for this recycling. For such tracking to be possible, however, it is necessary to consider the effect of pressure on the isotopic fractionation of chlorine.

This paper reports the results of a study of chlorine isotopic fractionation for the major chlorine-bearing minerals (i.e., apatite-group minerals, muscovite, phlogopite, tremolite, lizardite, marialite and metal halides) as a function of temperature and pressure. The main objective of the study was to quantify the extent of chlorine isotope fractionation among chlorine-bearing minerals in high-pressure (HP) and ultra-high pressure (UHP) environments, with the aim of assessing the factors controlling equilibrium chlorine isotope fractionation that might impact on the chlorine isotope heterogeneity of the mantle.

2. Calculation details

2.1. Mineral models

Common chlorine-bearing metamorphic minerals, namely apatite-group minerals (Cl-Ap, F-Cl-Ap, OH-Cl-Ap) ($Ca_5(PO_4)_3(F,Cl,OH)$), muscovite ($KAl_2(Si_3Al)O_{10}(OH)Cl$), phlogopite ($KMg_3(Si_3Al)O_{10}(OH)Cl$), tremolite ($Ca_2Mg_5Si_8O_{22}(OH)Cl$), lizardite ($Mg_3Si_2O_5(OH,Cl)_4$), marialite ($Na_4Al_3Si_9O_{24}Cl$) and metal halides (halite) (NaCl) are considered in this study. The mineral structures were built, based on the Material Studio Materials Visualizer module (Accelrys, Inc., version 7.0), with reference to the experimental lattice parameters from the American Mineralogist Crystal Structure Database (Downs and Hall-Wallace, 2003). The crystal structures of these minerals are illustrated in Fig. 2 and the modeling parameters are listed in Table 1. The chlorine content of the minerals considered (i.e., wt%) in our models, i.e., chlorapatite, fluoro-chlorapatite, hydroxyl-chlorapatite, muscovite, phlogopite, tremolite, lizardite, marialite and halite, was estimated to be 6.8%, 3.5%, 3.5%, 8.5%, 8.1%, 4.3%, 1.6-40.4%, 4.2% and 60.7%, respectively.

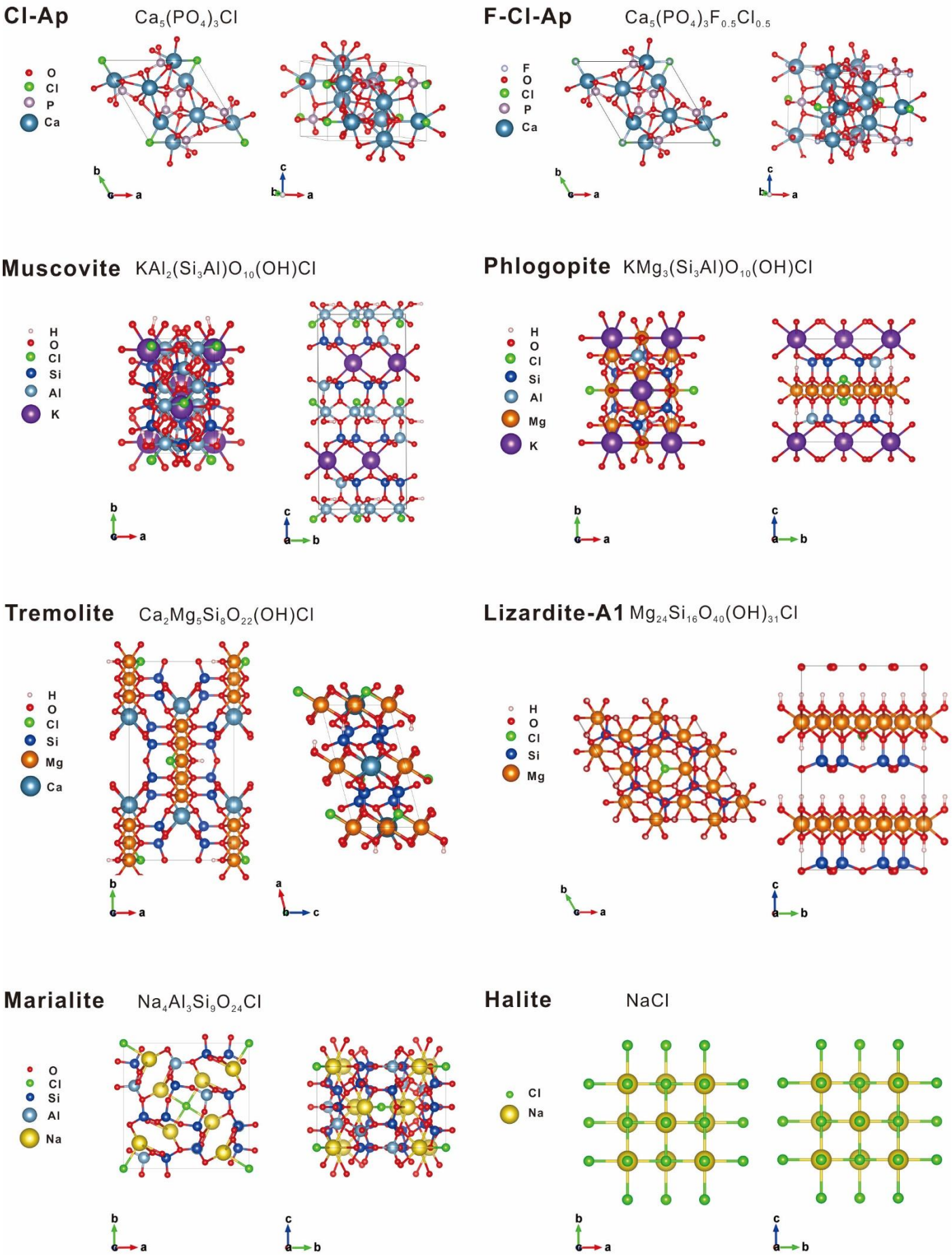
Cl-Ap
$Ca_5(PO_4)_3Cl$
O
Cl
P
Ca
F-Cl-Ap
$Ca_5(PO_4)_3F_{0.5}Cl_{0.5}$
F
O
Cl
P
Ca
Muscovite
$KAl_2(Si_3Al)O_{10}(OH)Cl$
H
O
Cl
Si
Al
K
Phlogopite
$KMg_3(Si_3Al)O_{10}(OH)Cl$
H
O
Cl
Si
Al
Mg
K
Tremolite
$Ca_2Mg_5Si_8O_{22}(OH)Cl$
H
O
Cl
Si
Mg
Ca
Lizardite-A1
$Mg_{24}Si_{16}O_{40}(OH)_{31}Cl$
H
O
Cl
Si
Mg
Marialite
$Na_4Al_3Si_9O_{24}Cl$
O
Cl
Si
Al
Na
Halite
NaCl
Cl
Na
a
b
c

Figure 2. A series of periodic boundary cell (PBC) models for minerals, presented as top and side views.

2.2. Calculation methods

A simplified approximation for estimating mass-dependent equilibrium isotopic fractionation given by Bigeleisen and Mayer (1947) is suitable for most substances, assuming that there is rigid rotation and harmonic vibration. For a chlorine isotope exchange reaction, if there is only one chlorine atom in substance X and *n* chlorine atoms in substance Y, this exchange reaction is:

$$nX + Y^* \leftrightarrow nX^* + Y \qquad \text{(Eq. 1)}$$

where X and Y identify the substances containing the lighter isotope (^{35}Cl), X* and Y* identify the substances containing the heavier isotope (^{37}Cl) and *n* is the number of chlorine atoms (^{37}Cl) substituted in Y*.

The isotope fractionation factor (α) for the general isotope exchange reaction between X and Y can then be written as (Liu and Tossell, 2005):

$$\alpha = \frac{\mathrm{RPFR(X)}}{\mathrm{RPFR}^{\frac{1}{n}}\mathrm{(Y)}} = \frac{\beta(\mathrm{X})}{\beta(\mathrm{Y})} \qquad \text{(Eq. 2)}$$

The harmonic approximation for the reduced isotopic partition function ratio (β factor) of X and Y is given by Eq. 3 below (Bigeleisen and Mayer, 1947; Kieffer and Werner, 1982; Dove, 1993; Schauble, 2004; Kowalski et al., 2013; Wu et al., 2015; Young et al., 2015; Li et al., 2017).

$$\beta = \frac{Q^*}{Q} = \left[\prod_{i=1}^{3N_{at}} \prod_q \frac{u^*_{q,i}}{u_{q,i}} \frac{\exp\left(-\frac{u^*_{q,i}}{2}\right)}{1-\exp\left(u^*_{q,i}\right)} \frac{1-\exp\left(u^*_{q,i}\right)}{\exp\left(-\frac{u^*_{q,i}}{2}\right)}\right]^{1/N_q N} \qquad \text{(Eq. 3)}$$

where Q is the vibrational partition function, the asterisk refers to the heavy isotope, subscript *i* is the number of vibrational modes and N_{at}, N_q, and N represent the number of atoms in a unit cell, phonon wave vectors, and sites of isotopes, respectively (Schauble et al., 2006; Blanchard et al., 2009; Li et al., 2017). The term $u_{q,i}$ ($u^*_{q,i}$) can be calculated using Eq. 4:

$$u_{q,i} = \frac{hc \cdot \upsilon_{q,i}}{kT} \qquad \text{(Eq. 4)}$$

where *h* is Plank's constant, *c* is the speed of light, $\upsilon_{q,i}$ is a harmonic vibrational frequency of the ith vibrational mode at a phonon wave vector *q*, *k* is Boltzmann's constant and *T* is temperature in degrees Kelvin.

The term β is a function of the unit cell volume, pressure and temperature, and can be expressed as a function of P and T in combination with the equation of state of $P(V,T) = \partial F(V,T)/\partial V$ (Huang et al., 2013; Wu et al., 2015). The quasi-harmonic approximation for the Helmholtz free energy, $F(V, T)$, is given by:

$$F(V,T) = U(V) + \sum_{qj} \frac{h\omega_{qj}(V)}{2} + K_B T \sum_{qj} \ln\left(1 - \exp\left[\frac{h\omega_{qj}(V)}{K_B}\right]\right) \qquad \text{(Eq. 5)}$$

where q is a wave vector in the first Brillouin zone, j is an index of the phonon mode with frequency ω_{qj}, and V and T are the volume and temperature of the system, respectively. The first, second, and third terms in Eq. 5 are the static internal, zero-point, and vibrational energy contributions, respectively. The relationships between the Helmholtz free energy and volume are expressed in terms of (or approximated by) the third-order Birch-Murnaghan finite-strain equations of state (Huang et al., 2013).

The Brillouin zone (BZ) was sampled with variable k-point preferentially following a rule of $a \times k1 \approx b \times k2 \approx c \times k3$ for geometry optimization. The energy cut-off for the plane wave basis was from 830 to 990 eV. The generalized-gradient approximation (GGA) method together with the exchange-correlation functional of Perdew, Burke and Ernzerhof (PBE) (Perdew et al., 1996), and norm-conserving pseudopotentials were employed in both geometric optimizations and phonon calculations for the PBC model of the chlorine-bearing minerals. The computation details for supercell size, total atoms per cell, cut-off energy, k-points, q-points and quality set are listed in Table 1. The calculations were carried out using the Cambridge Serial Total Energy Package (CASTEP) (Clark et al., 2005).

Table 1. Calculation sets for chlorine-bearing minerals

Minerals	Formula	Supercell	N_{atoms}	Cut-off energy (eV)	k-points	q-points	Quality
Chlorapatite	$Ca_5(PO_4)_3Cl$	1 × 1 × 1	42	880	2 × 2 × 2	4	Ultra-fine
		1 × 1 × 2	84	880	2 × 2 × 1	4	Ultra-fine
Fluoro-chlorapatite	$Ca_5(PO_4)_3F_{0.5}Cl_{0.5}$	1 × 1 × 1	42	940	2 × 2 × 2	4	Ultra-fine
Hydroxyl-chlorapatite	$Ca_5(PO_4)_3(OH_{1-x}Cl_x)$						

	$Ca_5(PO_4)_3(OH_{0.5}Cl_{0.5})$	1 × 1 × 1	43	880	2 × 2 × 2	4	Ultra-fine
	$Ca_5(PO_4)_3(OH_{0.75}Cl_{0.25})$	1 × 1 × 2	87	880	2 × 2 × 2	2	Ultra-fine
	$Ca_5(PO_4)_3(OH_{0.5}Cl_{0.5})$	1 × 1 × 2	86	880	2 × 2 × 1	4	Ultra-fine
	$Ca_5(PO_4)_3(OH_{0.25}Cl_{0.75})$	1 × 1 × 2	85	880	2 × 2 × 2	2	Ultra-fine
Muscovite	$KAl_2(Si_3Al)O_{10}(OH)Cl$	1 × 1 × 1	80	830	3 × 2 × 1	6	Ultra-fine
Phlogopite	$KMg_3(Si_3Al)O_{10}(OH)Cl$	1 × 1 × 1	42	990	3 × 2 × 1	12	Ultra-fine
Tremolite	$Ca_2Mg_5Si_8O_{22}(OH)Cl$	1 × 1 × 1	80	990	1 × 1 × 3	6	Ultra-fine
Lizardite-A0	$Mg_3Si_2O_5Cl_4$	1 × 1 × 1	14	990	3 × 3 × 2	8	Ultra-fine
Lizardite-A1	$Mg_{24}Si_{16}O_{40}(OH)_{31}Cl$	1 × 1 × 1	143	990	2 × 2 × 1	1	Ultra-fine
Lizardite-A2	$Mg_{24}Si_{16}O_{40}(OH)_{31}Cl$	1 × 1 × 1	143	990	2 × 2 × 1	1	Ultra-fine
Lizardite-A3	$Mg_{24}Si_{16}O_{40}(OH)_{30}Cl_2$	1 × 1 × 1	142	990	2 × 2 × 1	1	Ultra-fine
Marialite	$Na_4Al_3Si_9O_{24}Cl$	1 × 1 × 1	82	830	1 × 1 × 2	8	Ultra-fine
Halite	NaCl	1 × 1 × 1	8	830	3 × 3 × 3	36	Ultra-fine

Note: 'Quality' is a data quality control tab and used to limit parameter sets, such as K-points, Cut-off energy, and q-points. Generally, 'Ultra-fine' means the most accurate results at the expense of the longest calculation time provided by CASTEP.

K-points: used for Brillouin zone sampling; the magnitude of the error in the total energy can be reduced by using a denser set of k-points.

Cut-off energy: the periodic system (mineral model) is calculated with plane wave basis sets; a higher cut-off energy corresponds to the use of more plane waves to describe the system.

q-points: used in the real space dynamical matrix calculations to obtain a set of frequencies at each point.

2.3. Pressure ranges in the mineral computational setting

Apatite, which can be described by the general formula $A_5(XO_4)_3Z$, is a versatile mineral that can incorporate a diverse range of major and trace elements, including the halogens, in its structure and is stable over a wide range of P-T conditions (up to 7.5 GPa in subduction zones) (e.g., Pan and Fleet, 2002; Hughes and Rakovan, 2015; Andersson et al., 2019). The A-site accommodates large cations (e.g., Ca^{2+}, Sr^{2+}, Pb^{2+}, Ba^{2+}, Mg^{2+}, Mn^{2+}, Fe^{2+}, REE^{3+}, Eu^{2+}, Cd^{2+}, Na^{+}), and the X-site is occupied primarily by P^{5+} (as PO_4^{3+}), which is in IV-fold coordination (Piccoli and Candela, 2002). This site can also accommodate other small, highly-charged cations (e.g., Si^{4+}, S^{6+}, As^{5+}, V^{5+}) (Piccoli and Candela, 2002). The Z site is occupied by the halogens F^- and Cl^-, as well as by OH^-. The stability of apatite varies depending on the pressure and temperature. At 950 °C and a pressure of 7.5 GPa, OH-apatite breaks down to tuite { γ -$Ca_3(PO_4)_2$} (Konzett and Frost, 2009). This pressure limit on its

stability, however, increases with increasing temperature and between 1100 and 1300 °C, OH-apatite is stable up to a pressure of 12 GPa; the corresponding temperature for F-apatite is between 1300 and 1500 °C (Murayama et al., 1986). Consistent with these constraints, we have assessed the effect of pressure on the fractionation of chlorine isotopes between apatite and other phases for pressures from 0 to 10 GPa.

The effect of high pressure on the fractionation of chlorine isotopes between micas and other phases is of interest because micas are considered to be the main repository of water and alkali metals in the mantle, and therefore play a critical role in the genesis of magmas above subduction zones (e.g., Schmidt et al., 2004). Phlogopite has three octahedral cations that coordinate with the hydroxyl anion, and muscovite has two octahedral cations and a vacancy (Williams et al., 2012). The different coordination environments lead to differences in the vibrational response of the hydroxyl ion. The chlorine isotopic fractionation of muscovite {$KAl_2(Si_3Al)O_{10}(OH)Cl$} and phlogopite {$KMg_3(Si_3Al)O_{10}(OH)Cl$} was investigated for 0, 0.05, 0.5, 2.5 and 5.0 GPa, pressures that span the range for subducting crust.

Amphiboles show great compositional variability and are stable over a wide range of P-T conditions from those of the crust to the upper mantle (e.g., Green and Wallace, 1988; Comodi et al., 1991). Tremolite {$Ca_2Mg_5Si_8O_{22}(OH)Cl$} is a low-pressure amphibole, with silicon in tetrahedral coordination and only magnesium in octahedral coordination (Comodi et al., 1991). It can form as a result of a reaction involving dolomite, quartz and water that also produces calcite and carbon dioxide (Skippen, 1971). Kirby (1987) investigated the stability of polycrystalline tremolite by constructing a phase diagram corresponding to the bulk composition of tremolite and showed that tremolite is stable

up to a pressure of ~ 2.5 GPa. The pressure dependence of chlorine isotopic fractionation in tremolite was investigated for 0, 0.05, 0.5, 1.0 and 2.5 GPa.

Scapolite is a framework aluminosilicate of tetragonal symmetry that is stable over a wide range of P-T conditions and is observed mainly in metamorphic rocks (Baker and Newton, 1994). The generalized chemical formula for scapolite is $M_4[T_{12}O_{24}]A$, where M = Na and/or Ca, T = Si or Al, and A = Cl^- and/or CO_3^{2-}. The scapolite group comprises two members, marialite {$Na_4Al_3Si_9O_{24}Cl$; Ma} and meionite {$Ca_4Al_6Si_6O_{24}CO_3$; Me}, which form a continuous solid solution series (Bayliss, 1987). Most reports of marialite have been of occurrences in greenschist to eclogite facies, and in contact and retrograde metamorphic assemblages (Kullerud and Erambert 1999; Bernal et al., 2017; Lotti et al., 2018). Marialite of hydrothermal origin has been reported from a number of ore deposits (Almeida and Jenkins, 2017). In order to avoid the issue of the tetragonal-to-triclinic phase transition, which takes place at ca. 9.5 GPa (Lotti et al., 2018), chlorine isotope fractionation involving scapolite was investigated for pressures of 0, 0.05, 0.5, 2.5 and 5.0 GPa.

At ambient P-T conditions, halite crystallizes in the so-called rock salt structure, a cubic array of Na and Cl atoms in equal proportions (1:1 stoichiometry) with six-fold coordination. This structure is stable to relatively high pressure. A structural phase transition to the cubic, eight-fold coordinated NaCl-B2 phase is observed at ~30 GPa (Zhang et al., 2013). The chlorine isotope fractionation of halite was investigated over the pressure range from 0 to 10 GPa.

Serpentine {$Mg_3Si_2O_5(OH)_4$}, an alteration (hydration) product of olivine and pyroxene, is thought to be an important component of the descending slab (Ringwood, 1975; Gregory and Taylor, 1981; Meade and Jeanloz, 1991). Serpentine group minerals (e.g., lizardite, antigorite) are trioctahedral phyllosilicates, the structure of which is based on the stacking of a 1:1 layer composed of one

octahedral and one tetrahedral sheet (Wicks and O'Hanley, 1988). Lizardite, the most abundant serpentine mineral in the Earth's upper crust, has the most straightforward structure, and is the standard for comparison in estimating the structures of the other serpentine group minerals (Dódony and Buseck, 2004). The powder X-Ray diffraction patterns from lizardite samples at high pressure and room temperature show that the crystal structure of serpentine is gradually eliminated by compression above 6.6 GPa (Meade and Jeanloz, 1990, 1991). In order to increase the database of thermodynamic properties of serpentine, Hilairet et al. (2006) determined the P-V Equations of State (EoS) of lizardite and chrysotile at ambient temperature up to 10 GPa, by in situ synchrotron X-Ray diffraction in a diamond-anvil cell. Neither amorphization or hysteresis was observed during compression and decompression, and no phase transition was resolved for lizardite. Experiments by Capitani and Stixrude (2012) failed to detect a tetrahedral bulk modulus for lizardite at pressures of 7-23 GPa, although an elastic anomaly was predicted to be present at about 6 GPa in a first-principles density functional calculation based on the structure, elasticity, and vibrational properties of lizardite (Tsuchiya, 2013). In order to study pressure-dependent chlorine isotopic fractionation in lizardite, we used the P31m space group and atomic positions from the Lizardite 1T polytype {$Mg_3Si_2O_5(OH)_4$} (Mellini and Viti, 1994). In this paper, four different models for lizardite have been considered to better assess the influences of chlorine substitution of inner and inter-layer OH sites and the chlorine content on the calculated reduced partition function ratios for $^{37}Cl/^{35}Cl$ in lizardite, as described below: (i) Lizardite-A0 is a unit cell where all the hydroxyl groups were replaced by Cl atoms, with the chemical formula of $Mg_3Si_2O_5Cl_4$ and Cl% of 40.4%; (ii) Lizardite A1, A2 and A3 were built from supercells, replacing one inner OH by one Cl atom for A1 with Cl% of 1.6%, one inter-layer OH by one Cl atom for A2 with Cl% of 1.6%, and one inner OH and one inter-layer OH by two Cl atoms for A3 with Cl%

of 3.1%. The number of total atoms in individual A1, A2 and A3 supercells is 143, 143, 142, respectively. As the supercells Lizardite A1, A2, and A3 are more appropriate to represent the natural mineral, the P-T dependence of reduced partition function ratios for $^{37}Cl/^{35}Cl$ in lizardite was estimated based on the computational results from the models of Lizardite A1, A2, and A3 in this study. The pressure dependence of chlorine isotopic fractionation in lizardite was investigated for 0, 0.05, 0.5, 2.5 and 5.0 GPa.

2.4. Error estimation

The calculation accuracy of β-factor values depends primarily on two factors, the uncertainty associated with the calculated phonon frequencies between isotopomers using density functional perturbation theory (DFPT) and the uncertainty related to anharmonic effects (Méheut et al., 2007). The uncertainty in the calculation of phonon frequencies by DFT, at the PBE level, leads to a systematic relative error of about 5%, which is similar to that affecting the calculation of β-factors. The uncertainty arising from anharmonic effects in minerals is relatively small, whereas there is strong anharmonic effect for water leading to a relative error of -5% (Méheut et al., 2007). The relative error associated with the calculation of the phonon frequency in this study is estimated to be ±4% (Fig. S1), which is similar to that obtained by Méheut et al. (2007). Consequently, the relative error for the β factor and that for the fractionation factor ($\Delta_{A-B} = 1000\ln\alpha_{A-B}$) of the minerals are estimated to be ±4% and ±8%, respectively. The overall absolute errors for $\Delta_{lizardite-halite}$ are ±0.41‰, ±0.11‰, ±0.04‰ at 300 K, 600 K and 1000 K, respectively.

3. Results

3.1. Equilibrium chlorine isotope fractionation at ambient conditions

To assess the accuracy of the theoretical estimates, the calculated lattice parameters and vibrational frequencies of the minerals mentioned above were compared to their experimentally determined values (Table S1, Fig. 3). The good agreement between the two sets of data shows that the PBE functional and norm-conserving pseudopotentials can be used to reliably predict the isotopic fractionation of chlorine between pairs of these minerals.

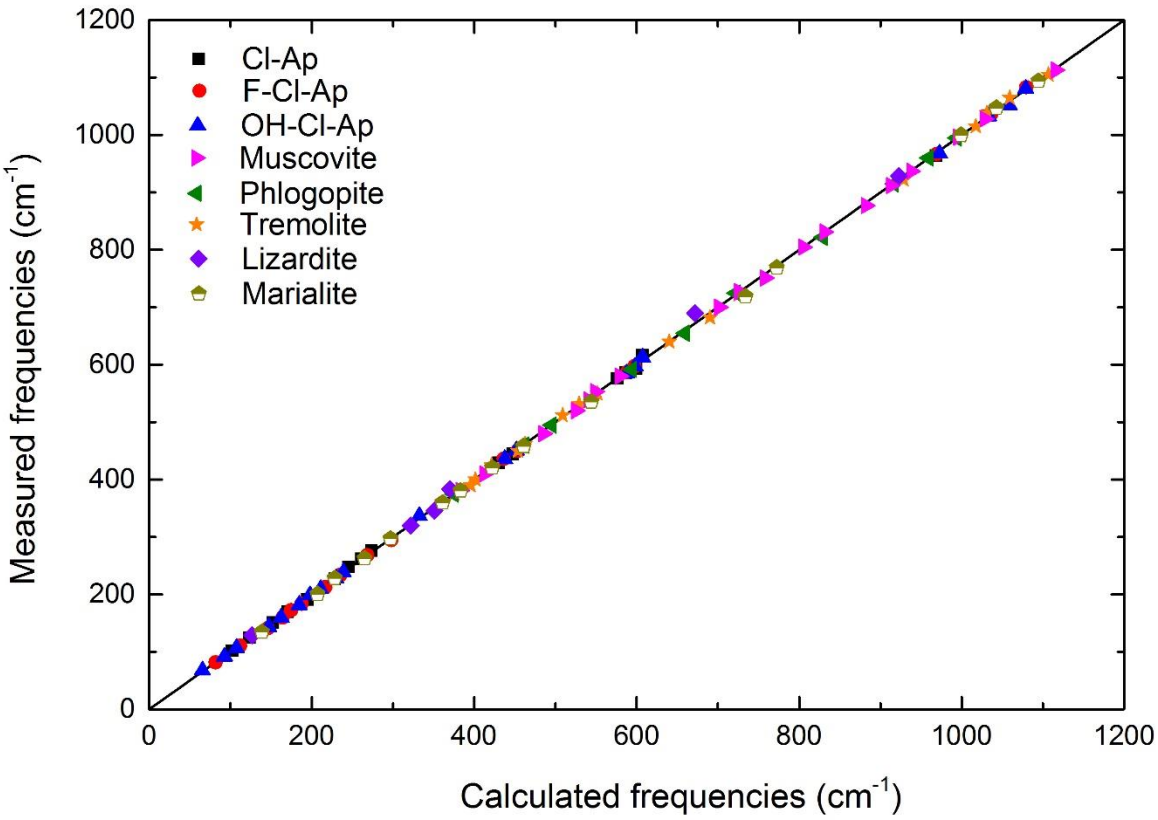

Figure 3. Comparison of calculated and experimentally determined vibrational frequencies for chlorine-bearing minerals. The measured vibrational frequencies are from previous studies, as listed in Table S2 in the Appendix.

The calculated reduced partition function ratios (1000lnβ) for chlorine-bearing minerals at 0 GPa are shown in Fig. 4. The values of 1000lnβ for $^{37}Cl/^{35}Cl$ decrease in the order phlogopite > muscovite >

tremolite > lizardite > fluoro-chlorapatite > hydroxyl-chlorapatite > chlorapatite > sodium chloride > marialite. The β values for halite, chlorapatite and lizardite estimated in this study were compared to those calculated by Schauble et al. (2003) and Balan et al. (2019) for the temperature range, 300 K to 1000 K (Fig. 4). Balan et al. (2019) built a unit-cell of the periodic model of lizardite with a 2×2×2 supercell containing 112 atoms, and satisfactorily reproduced the chlorine substitution for sites at an inner-OH or an inter-layer OH. The β values of lizardite A0 determined in the current study are close to those for the lizardite Cl2 reported by Balan et al. (2019); at 450 K the difference is 0.07‰ and at 800 K it is 0.01‰. Furthermore, the differences in the β values of lizardite A2 (this study) and lizardite Cl1 (Balan et al., 2019) are negligible, e.g., 0.004‰ at 450 K (Fig. 4). In addition, comparisons for other minerals, such as halite and chlorapatite, show that the difference in the β values are less than 0.5‰ at 300 K and is even smaller, ~0.1‰ at 600 K; the latter might be due to a computational error for β factors of minerals obtained using different exchange-correlation functionals. At ambient P-T conditions, the 1000lnβ factors correlate negatively with the metal-Cl bond length of the minerals (Fig. 5a). The same observation was made for the equilibrium fractionation of Ca isotopes (Huang et al., 2019). Minerals containing trivalent metals (e.g., Al^{3+}) with short bonds between these metals and chlorine were shown to have higher β factors than minerals with monovalent metal ions (e.g., Na^{+}) and long bonds between these cations and Cl. The β factors of minerals in which Cl is bonded to Mg (lizardite, phlogopite and tremolite) are similar, as are the β factors for minerals in which Cl is bonded to Ca (apatite group minerals). These observations are in excellent agreement with those for chlorine isotopic fractionation reported by Schauble et al. (2003) and Balan et al. (2019). In order to evaluate the correlation of β factors with the cation-chlorine bond strength of the minerals studied, we calculated the latter using the relationship:

$$C_{ct-Cl} = \frac{V}{(r_{ct}+r_{Cl})CN_{ct}} \qquad \text{(Eq. 6)}$$

where $C_{ct\text{-}Cl}$ is the cation-chlorine bond strength, CN_{ct} is the coordination number of the cation, r is the ionic radius of the cation and chloride and V is the oxidation state of the cations (Zheng, 1996). With the exception of muscovite, the 1000lnβ values correlate positively with the metal-Cl bond strength of these minerals (Fig. 5b). The reason for the anomalous behavior of muscovite is unclear but might be due to the polarization effect of Al^{3+} ions.

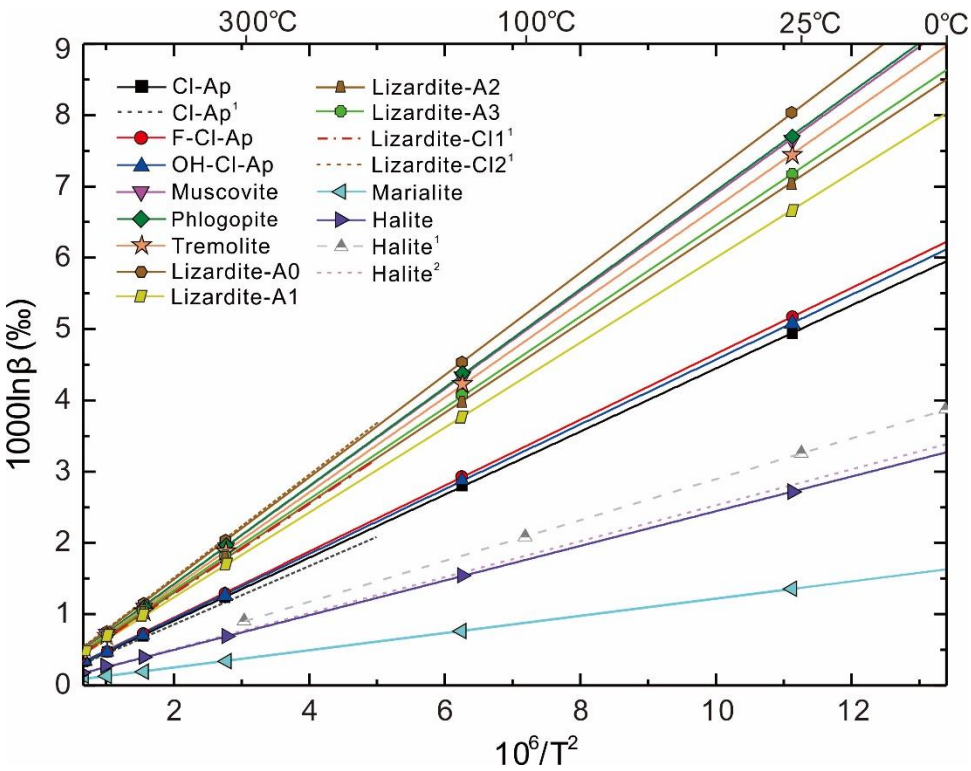

Figure 4. Temperature dependence of the equilibrium reduced partition function ratios 10^3lnβ for chlorine isotopes in chlorine-bearing minerals at 0 GPa. The data for halite[1] are from Schauble et al. (2003). The data for Cl-Ap[1], halite[2] and lizardite-Cl1/Cl2[1] are from Balan et al. (2019).

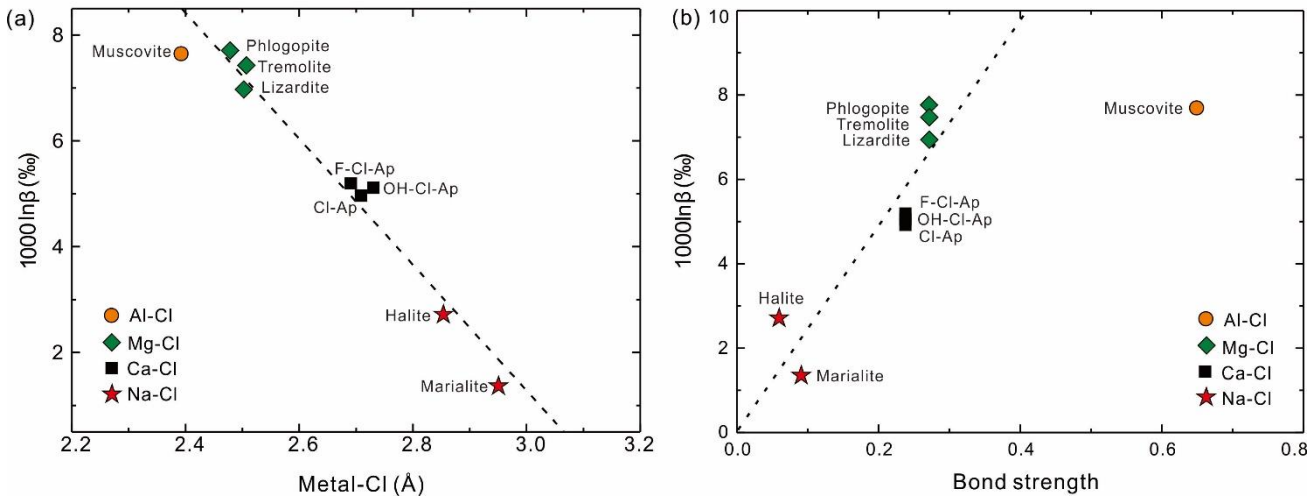

Figure 5. Equilibrium reduced partition function ratios $10^3 \ln\beta$ as a function of the metal-Cl bond length (a) and the metal-Cl bond strength based on Eq. 6 (b) in chlorine-bearing minerals at ambient P-T conditions.

Based on the results of a first-principles calculation, the Ca and Mg concentrations in orthopyroxene and carbonate minerals are highly sensitive to the lengths of the metal-O bond (Feng et al., 2014; Wang et al., 2017). To better understand the solid-solution properties and ordering scheme affecting chlorine isotope fractionation in OH-F-Cl apatite, we examined the effect of Cl concentration on the Ca-Cl bond length and equilibrium fractionation of chlorine isotopes among apatite group minerals ($Ca_5(PO_4)_3((F,Cl)_xOH_{1-x})$). As shown in Fig. 6, the 1000lnβ factors decrease linearly with increasing *x* (i.e., Cl content) from 1/4 to 3/4, and then increase slightly as *x* approaches unity. A reverse trend for the average Ca-Cl bond length versus. *x* is also observed, confirming that the strength of the Ca-Cl bond exerts an important control on the equilibrium fractionation of chlorine isotopes in apatite group minerals. Considering the relatively large difference of 0.61‰ in 1000lnβ at 300 K, the chemical composition of apatite group minerals should be taken carefully into account in interpreting low-temperature geochemical processes.

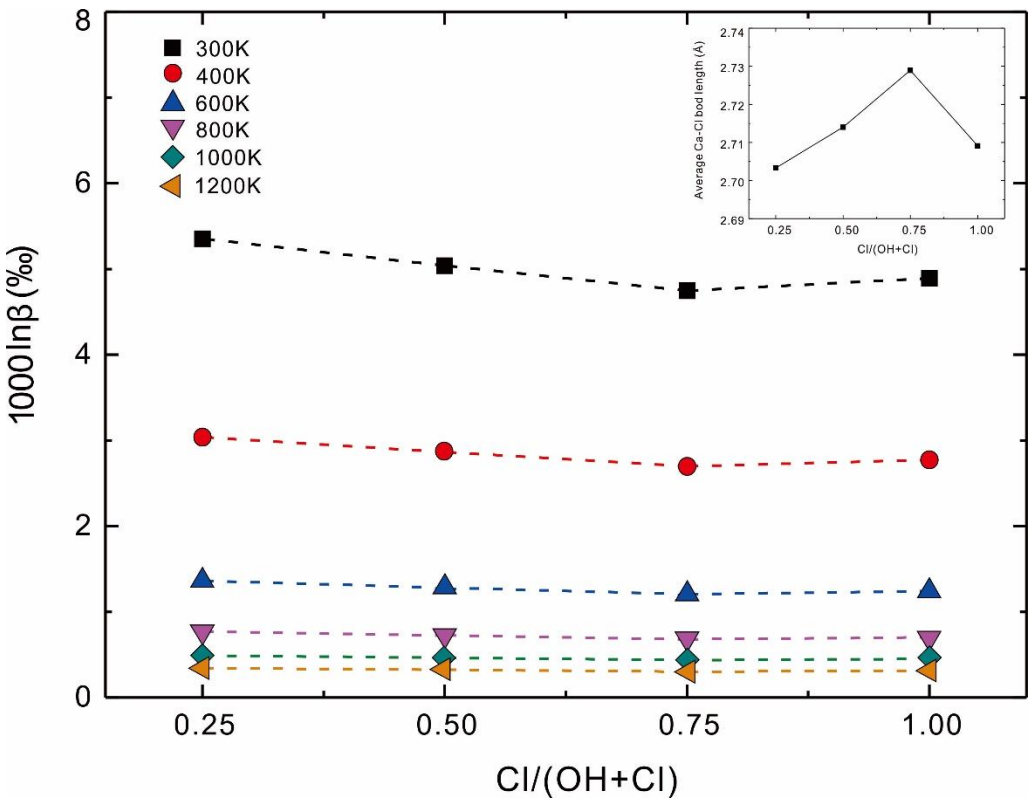

Figure 6. The dependence of $10^3 \ln\beta$ of apatite group minerals on Cl/(OH+Cl) at various temperatures. The insert shows the average Ca-Cl bond length versus Cl/(OH+Cl) at ambient P-T conditions.

3.2. Pressure effects on chlorine isotope fractionation in minerals

The effect of pressure on chlorine isotope fractionation is of interest because all of the minerals investigated in this study are stable over wide ranges of pressure. As shown in Fig. S2, the unit cell volume of each mineral decreases and the density increases with increasing pressure. The calculated slope of unit cell volume versus pressure for apatite and lizardite is approximately the same as that obtained experimentally by Comodi et al. (2001), Mellini and Zanazzi (1989) and Hilairet et al. (2006), indicating the robust nature of our theoretical calculations.

The average Ca-Cl, Na-Cl, Mg-Cl and Al-Cl bond lengths in several chlorine-bearing minerals are shown as a function of pressure in Fig. 7. In general, the metal-chlorine bond length decreases with increasing pressure, but the slopes are not all uniform. The slope for the Na-Cl bond length in marialite becomes increasingly negative above 2.5 GPa, whereas the slope for the Ca-Cl bond length of

hydroxyl-chlorapatite remains almost constant at pressures greater than 5 GPa. Slopes for the metal-Cl bond lengths of muscovite, phlogopite and tremolite decrease slightly with increasing pressure.

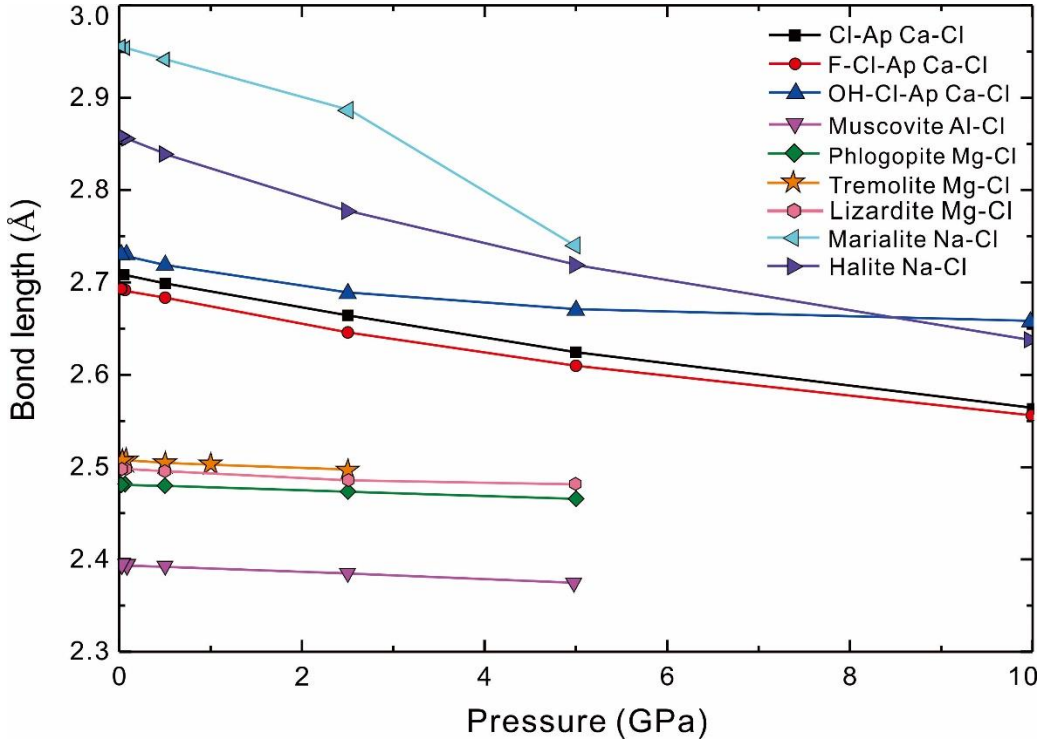

Figure 7. Variations in the average metal-Cl bond length for chlorine-bearing minerals with increasing pressure at static conditions.

4. Discussion

4.1. P-T dependence of chlorine isotope fractionation among chlorine-bearing minerals

At 300 K, the differences in 1000lnβ values for chlorine isotopes at 10 GPa relative to those at ambient pressure are 3.13‰ (fluoro-chlorapatite), 3.06‰ (chlorapatite) and 2.02‰ (hydroxyl-chlorapatite) (Fig. 8, Table S3), showing that fluoro-chlorapatite is the most pressure-sensitive member of the apatite group. Halite is the most pressure-sensitive of all the minerals considered with a difference in its 1000lnβ value at 10 GPa relative to ambient pressure of 3.30‰. At 800 K and 2.5 GPa, the calculated reduced partition function ratios (lnβ) follow the sequence, muscovite > phlogopite >

tremolite > lizardite > fluoro-chlorapatite > chlorapatite > hydroxyl-chlorapatite > halite > marialite, whereas the sensitivity to pressure ($10^3\ln[\beta_p/\beta_0]$) follows the sequence, halite > fluoro-chlorapatite > chlorapatite > marialite > hydroxyl-chlorapatite > lizardite > tremolite > muscovite > phlogopite.

An expression for the β-factors of the above minerals, based on their thermodynamic properties, was derived using the first-order thermodynamic perturbation theory of Polyakov and Kharlashina (1994) expressed in Eq. 7:

$$\left(\frac{\partial\beta}{\partial P}\right)_T = \frac{\gamma_{th}}{B_T}\left[(\beta - 1) + \frac{\Delta m}{m^*}\frac{C_V - 3R}{2R}\right] \qquad \text{(Eq. 7)}$$

where γ_{th} is the thermal Grüneisen parameter, which depends only slightly on temperature and is essentially independent of pressure, B_T is the isothermal bulk modulus expressed as $B_T = -\left(\frac{\partial lnV}{\partial P}\right)_T^{-1}$, C_V is the molar heat capacity of a crystal, m and m^* are the masses of the light and heavy isotope atoms and $\Delta m = m^* - m$ and R is the gas constant.

The effect of pressure on the equilibrium isotope fractionation factors is due to i) a difference in the thermal Grüneisen parameter (γ_{th}) of the minerals, ii) differences in the values of the derivatives $\frac{\partial\beta}{\partial P}$; and iii) differences in the isothermal bulk moduli (Polyakov and Kharlashina, 1994). Given that γ_{th} and C_V are constants for a particular mineral, and that B_T is a linear function of P (i.e., $B_T = a + bP$) (Polyakov and Kharlashina, 1994), integration of Eq. 7 gives the following expression:

$$ln\frac{\left(\beta - 1 + \frac{\Delta m}{m^*}\frac{C_V - 3R}{2R}\right)}{\left(\beta_0 - 1 + \frac{\Delta m}{m^*}\frac{C_V - 3R}{2R}\right)} = \frac{\gamma_{th}}{b}\ln\left(1 + \frac{b}{a}P\right) \qquad \text{(Eq. 8)}$$

As a is generally >> b (Polyakov and Kharlashina, 1994) and the term of $\frac{\Delta m}{m^*}\frac{C_V - 3R}{2R}$ is << 1, Eq. 8 can be simplified as:

$$ln\frac{(\beta - 1)}{(\beta_0 - 1)} = A + \gamma_{th}\frac{1}{a}P \qquad \text{(Eq. 9)}$$

This equation (Eq. 9) predicts a linear dependence of the β-factors on pressure, as has been shown in this study for $^{37}Cl/^{35}Cl$ in chlorine-bearing minerals (Fig. 8), and also for the β-factors for D/H in

brucite (Horita et al., 2002). Quantitative expressions for 1000lnβ as functions of pressure at low temperature (300 K) and high temperature (1000 K) are listed in Table S3. The theoretical predictions indicate that pressure-induced shifts cannot be ignored in interpreting stable chlorine isotopic ratios. Similar pressure effects have been reported for Mg isotope fractionation among garnet, clinopyroxene, orthopyroxene, and olivine, for O isotope fractionation between rutile and calcite, for C isotope fractionation among graphite, calcite and diamond, and H isotope fractionation in the brucite-water system (Huang et al., 2013; Polyakov and Kharlashina, 1994; Horita et al., 2002).

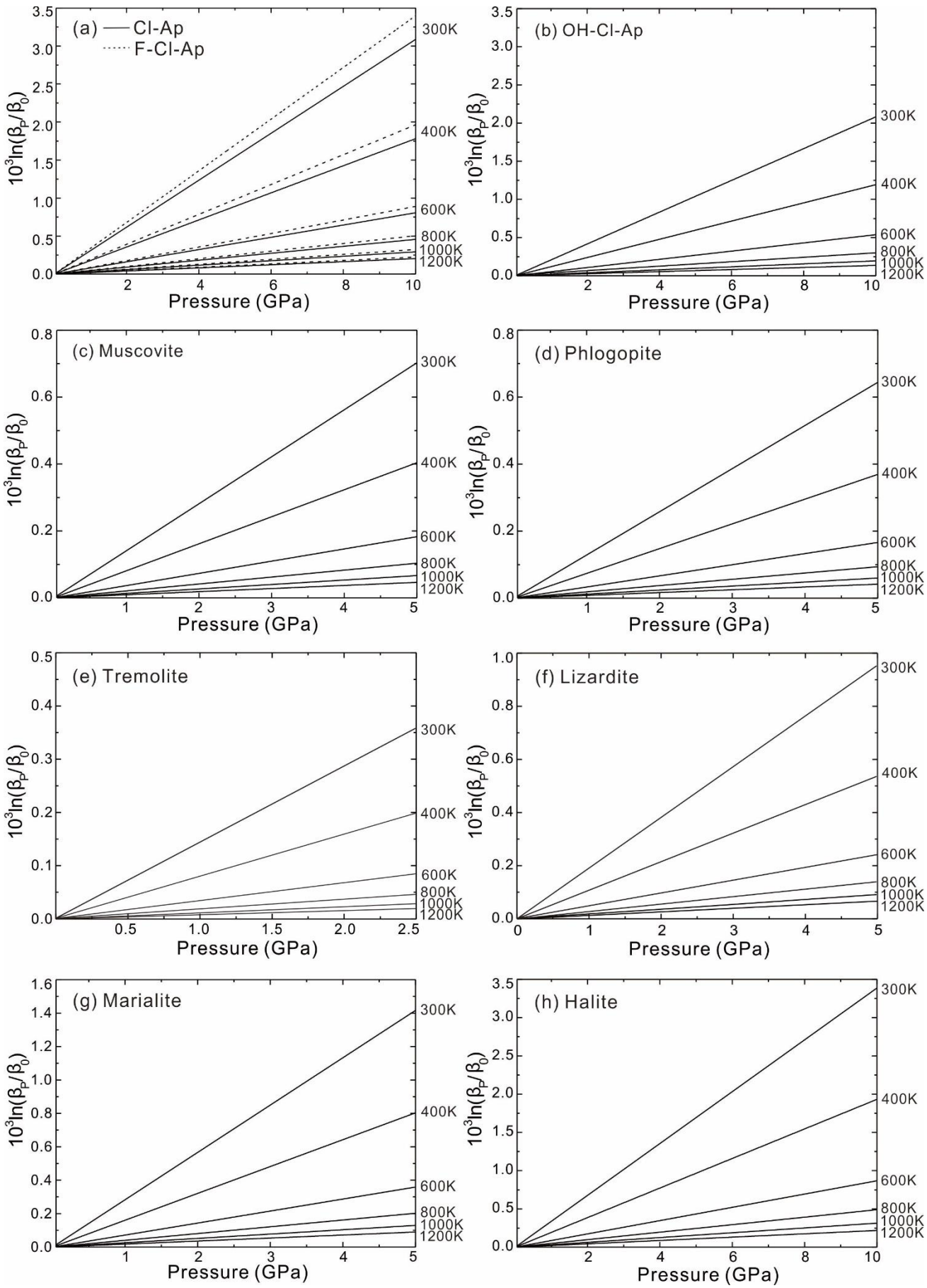
(a) Cl-Ap
F-Cl-Ap
(b) OH-Cl-Ap
(c) Muscovite
(d) Phlogopite
(e) Tremolite
(f) Lizardite
(g) Marialite
(h) Halite
300K
400K
600K
800K
1000K
1200K
Pressure (GPa)
$10^3\ln(\beta_P/\beta_0)$

440

Figure 8. The dependence of the reduced partition function ratios, $10^3\ln(\beta_p/\beta_0)$, on pressure for the $^{37}Cl/^{35}Cl$ ratio of chlorine-bearing minerals (apatite, muscovite, phlogopite, tremolite, lizardite, marialite, halite) as a function of pressure. The term β_0 represents the calculated reduced partition function at 0 GPa.

Fig. 9a illustrates the calculated Cl isotope fractionation ($\Delta^{37}Cl_{A\text{-}B} = 1000\ln\beta_A - 1000\ln\beta_B$) between Cl-bearing minerals (A) and halite (B) as a function of reciprocal temperature for 0 and 2.5 GPa, and provides insights into the equilibrium chlorine isotope fractionation among cogenetic chlorine-bearing minerals. Except for marialite, the values of $\Delta^{37}Cl_{A\text{-}B}$ are positive at 0 and 2.5 GPa. At conditions of sedimentary rock formation (300 K, 1×10^{-4} GPa), the value of $\Delta^{37}Cl_{fluoro\text{-}chlorapatite\text{-}NaCl}$ is about +2.5‰. In contrast, a $\Delta^{37}Cl_{fluoro\text{-}chlorapatite\text{-}NaCl}$ value of ~ +0.20‰ is estimated for the conditions at which fluoro-chlorapatite was intergrown with NaCl in carbonatite-hosted melt inclusions (1200 K, 2.5 GPa) (Kamenetsky et al., 2015).

4.2. P-T dependence of chlorine isotope fractionation between chlorine-bearing mineral and aqueous chloride

Previous studies have demonstrated that the pressure dependence of Li and B isotope fractionation in aqueous fluids matches well the shifts of pressure-induced vibrational frequencies (Kowalski and Jahn, 2011; Kowalski et al., 2013). Using the measured vibrational frequency shifts of the $Cl^{-}\cdots O\text{-}H$ stretching band in NaCl solution with pressure (Wang et al., 2013), we derived the relative shifts in the (β-1) factor employing the relationship of $(\beta - 1) \propto \upsilon^2 \sim \upsilon_0^2 + 2\upsilon_0 \Delta \upsilon$ (Schauble, 2004). As shown in Fig. S3, the calculated (β -1) values for aqueous chloride show a linear dependence on pressure in the range from 0.1 to 3.12 MPa, (β -1) = 1.55-0.013*P* (MPa)‰, and then remain almost constant at higher pressure (> 3 MPa) and ambient temperature. It therefore follows that the pressure

effect on chlorine isotope fractionation in aqueous fluids is insignificant and can be neglected at high temperature.

Based on the experimental results of Eggenkamp et al. (1995), Schauble et al. (2003) estimated values of 2.1-3.0‰ for $1000\ln\beta_{brine}$ and a value of +0.26‰ for $\Delta^{37}Cl_{halite\text{-}aqueous\ Cl}$ at 295 K, which is lower than the 1000lnβ value of 3.13 for aqueous chloride from the calculations of Czarnacki and Halas (2012). With reference to the median value of 2.55 for 1000lnβ in aqueous chloride at 295 K by Schauble et al. (2003), the over-estimates of $1000\ln\beta_{Cl^-}$ by Czarnacki and Halas (2012) were corrected by following the procedure of Rustad et al. (2010) and Kowalski et al. (2013). Assuming that 1000lnβ $\propto T^{-2}$ and a value of Δ1000lnβ of -0.58‰ as the difference between the 1000lnβ values of Schauble et al. (2003) and Czarnacki and Halas (2012) at 295 K, the 1000lnβ values reported by Czarnacki and Halas (2012) were overestimated by $\Delta 1000\ln\beta = (-0.58) \times (\frac{295}{T})^2$‰. The value of 1000lnβ of Czarnacki and Halas (2012) so corrected is plotted in Fig. S4. The temperature dependence of $10^3\ln\beta_A$-$10^3\ln\beta_B$ for $^{37}Cl/^{35}Cl$ between different chlorine-bearing minerals and aqueous chloride were derived as shown in Fig. 9b. This enables the $\delta^{37}Cl$ values of individual minerals equilibrating with aqueous fluid at different P-T conditions to be determined. For example, the data predict that the $\delta^{37}Cl$ value of fluoro-chlorapatite on the seafloor that is in isotopic equilibrium with seawater ($\delta^{37}Cl_{SMOC}$ of 0.0‰) is ~ +2.7‰. In contrast, chlorapatite crystallizing from a hydrothermal fluid containing chloride with a $\delta^{37}Cl$ value of 0‰ would have a $\delta^{37}Cl$ value of +0.63‰ at 600 K and 30 MPa. The $\delta^{37}Cl$ values in mantle minerals are more difficult to predict, as addressed below.

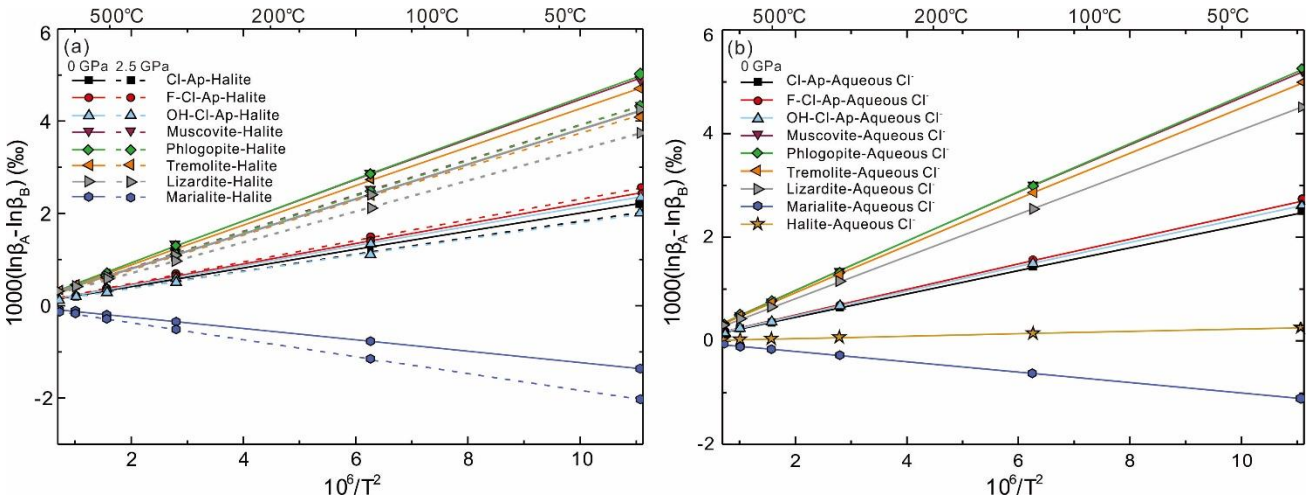

Figure 9. (a) Temperature dependence of $10^3\ln\beta_A$-$10^3\ln\beta_B$ for $^{37}Cl/^{35}Cl$ between different chlorine-bearing minerals (A) and halite (B) at 0 and 2.5 GPa. The solid lines are for 0 GPa and the dotted lines for 2.5 GPa. (b) Temperature dependence of $10^3\ln\beta_A$-$10^3\ln\beta_B$ for $^{37}Cl/^{35}Cl$ between different chlorine-bearing minerals (A) and aqueous chloride (B) at ambient pressure.

4.3. Controls on chlorine isotope heterogeneity in the mantle

4.3.1. Chlorine isotope heterogeneity in minerals in subduction-zones

As discussed in the introduction to this paper, the $\delta^{37}Cl$ values of mantle-derived materials are characterized by extreme heterogeneity as deduced from MORB, OIB and mantle xenoliths, for which the values range from -1.9‰ to +3.0‰. However, as mentioned above, whether the subduction of crustal materials into the mantle is partly or wholly responsible for this extreme $\delta^{37}Cl$ heterogeneity is still strongly debated.

From Fig. 9a, it is evident that the $\Delta^{37}Cl_{mineral\text{-}NaCl}$ values for apatite, tremolite and phyllosilicates (muscovite, phlogopite, lizardite) increase with decreasing temperature at pressures of 0-2.5 GPa; they are positive up to at least 1200 K. Greenschist-facies grade alteration due to hydrothermal circulation of seawater extends to a depth of ~3.5 km in MORB crust, beneath a water column 2.6 to 4 km in depth. With reference to the lithostatic pressure of ca. 0.17 GPa at this depth (Petrini and Podladchikov,

2000), values of $\Delta^{37}Cl_{mineral\text{-}NaCl}$ for tremolite, phyllosilicates and apatite range from +0.56 to +1.33‰ at 0.17 GPa and 600 K (a likely temperature for the alteration).

At the conditions of subduction illustrated in Fig. S5 (for example, 1300K and > 2.5 GPa), the values of $\Delta^{37}Cl_{mineral\text{-}NaCl}$ for tremolite, phyllosilicates and apatite are small, < +0.31‰. As the pressure effect is negligible at high temperature, the value of $\Delta^{37}Cl_{NaCl\text{-}aqueous\ Cl}$ in supercritical NaCl-H_2O at 1200 K was estimated to be +0.01‰. Assuming the processes reach equilibrium and the fluids present during HT to UHT metamorphism have $\delta^{37}Cl$ values close to SMOC ($\delta^{37}Cl$ = 0.0‰), secondary Cl-bearing minerals formed under these conditions would have small positive values of $\delta^{37}Cl$ (e.g., +0.34‰ for tremolite in a shallow subduction zone and +0.38‰ for phlogopite in a deep subduction zone). The predicted $\delta^{37}Cl$ values of fluoro-chlorapatite, muscovite and marialite in various metamorphic facies are shown in Fig. 10. The $\delta^{37}Cl$ values of fluoro-chlorapatite in the greenschist and garnet-ecologite facies are estimated to be +0.26‰ and +0.74‰, respectively, and those of muscovite in the lawsonite-eclogite and amphibolite facies to be +0.48‰ and +0.67‰, respectively. By contrast, the $\delta^{37}Cl$ values of marialite are slightly negative, -0.16‰ and -0.12‰ in the amphibolite and granulite facies, respectively.

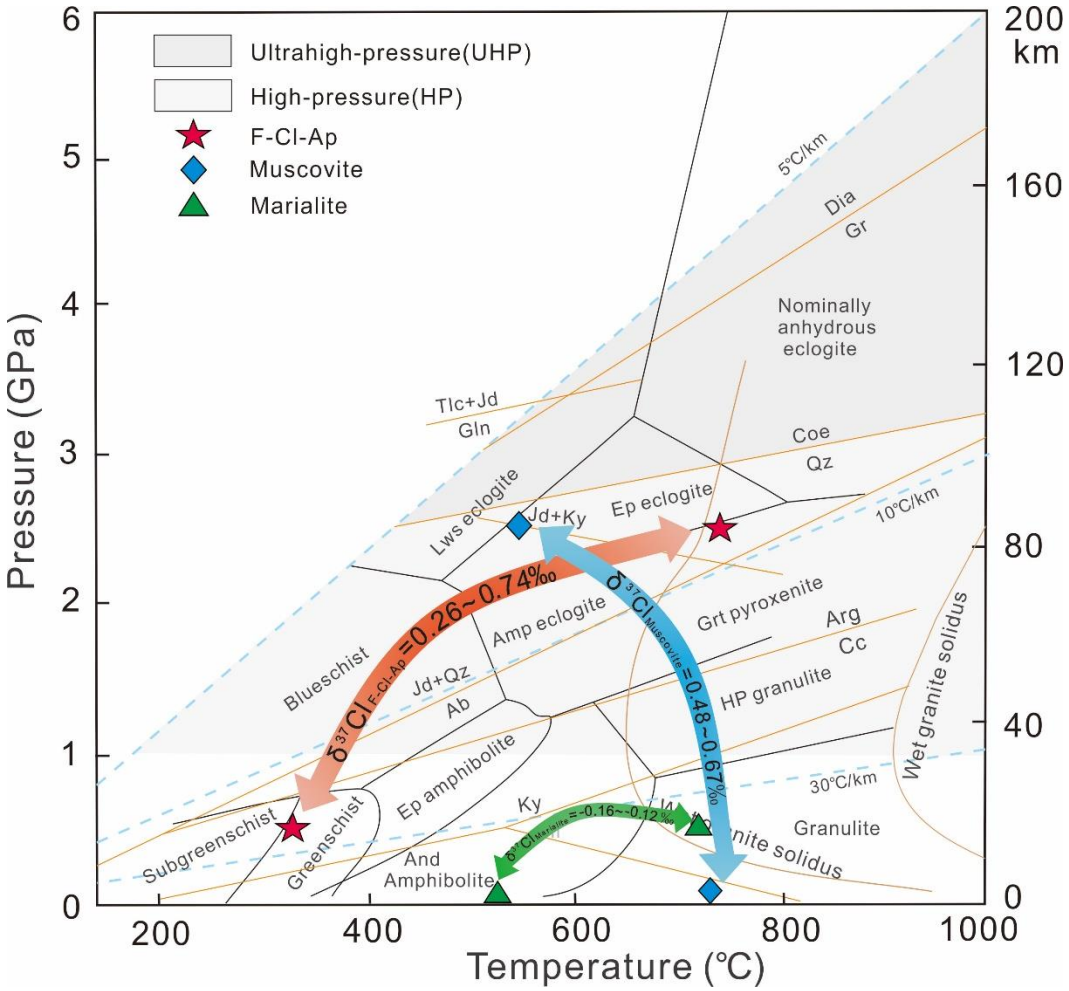

Figure 10. The δ^{37}Cl values of hydrous minerals in different metamorphic facies including those of subduction-zones. The dark-grey area corresponds to UHP metamorphism above the coesite/quartz transition boundary, whereas the light-grey area denotes HP metamorphism below the coesite/quartz transition line (modified after Zheng and Chen, 2017).

The data presented above indicate that variations in the δ^{37}Cl values of hydrous minerals during metamorphism are relatively minor over a wide range of P-T conditions. For the purpose of the current study, the simplest assumption is that the chloride in the subducting MORB has δ^{37}Cl values close to SMOC, although it should be noted that alteration of MORB as a result of interaction with seawater during seafloor spreading may locally affect its δ^{37}Cl value substantially. During the subduction of crustal rocks, however, aqueous fluids are generated not only by the prograde breakdown of hydrous minerals but also by the exsolution of molecular water and structural hydroxyl from nominally

anhydrous minerals (NAMs) (Zheng, 2009; Zheng and Hermann, 2014). As water is highly incompatible during partial melting of crust and mantle rocks (Zheng and Hermann, 2014) and chloride has a strong preference for the fluid over the melt, fluids enriched in chloride with variable δ^{37}Cl signatures participate extensively in metamorphism. It is also important to consider the contribution of sediments in evaluating chlorine incorporation in mantle materials during subduction. This is because the chlorine flux from sediments and pore water is twice that of oceanic crust during subduction (Eggenkamp, 2014). For the reasons given above, chlorine isotopic fractionation may be considerable as a result of the exchange of chloride between minerals and fluid in shallow and deep subduction zones (as shown schematically in Figure 11a). Indeed, the δ^{37}Cl values of minerals originating from hydrothermally altered MORB may range from +1 to +3‰. We distinguish between a primary mantle with a low Cl content and a secondary mantle fertilized by subduction that has a much higher chlorine content. From the data of Eggenkamp (2014), it is evident that the secondary mantle, with a higher chlorine content, is characterized by higher δ^{37}Cl values. This observation is consistent with the theoretical predictions from this study that the minerals undergoing metamorphism during subduction are enriched in ^{37}Cl relative to the metamorphic fluid. In contrast, subduction of sediments with the original δ^{37}Cl signatures of -8‰ to 0‰ to deep subduction zones may might produce δ^{37}Cl from -7‰ to +1‰.

4.3.2. Estimation of δ^{37}Cl for the bulk mantle

A δ^{37}Cl value for the bulk mantle can be estimated via mass balance, from the concept of the chlorine cycle and the annual Cl isotopic fluxes from continental crust, oceanic crust, ocean, sediments and mantle (Fig. 11b) using the following equation:

$$\{(\delta^{37}Cl_{OC} \times F_{OC-Mantle} + \delta^{37}Cl_{SP} \times F_{SP-Mantle}) - \delta^{37}Cl_{Mantle}(F_{Mantle-CC} + F_{Mantle-Ocean} + F_{Mantle-OC})\} \times t = \delta^{37}Cl_{Mantle} \times m_{Cl\ in\ Mantle} \quad \text{(Eq. 10)}$$

where $F_{A\text{-}B}$ is the annual flux of Cl from Reservoir A to Reservoir B, 10^9 kg·year^{-1}; $m_{Cl\ in\ mantle}$ is the total mass of Cl in mantle reservoir, 6.59×10^{19} kg (McDonough, 2000); *t* is the period of the chlorine cycle from the mantle to the surface reservoir. The abbreviations of OC, CC and SP represent ocean crust, continental crust and sediment and pore water.

Hay et al. (2006) prepared a detailed inventory of all evaporites deposited since the Ediacaran and concluded that there have been significant changes in the mean salinity of the ocean and that it declined progressively during the Phanerozoic. In applying Eq. 10, we have defined *t* as the beginning of the Ediacaran at ca. 635 Ma, a time when a large amount of chlorine began to flow from the mantle to the surface reservoir. Based on the δ^{37}Cl values reported for sediment and pore water (−8‰ to 0‰), and oceanic crust (-2‰ to 0‰) (Barnes and Sharp, 2017), and the annual fluxes of chlorine among those reservoirs (Eggenkamp, 2014), the δ^{37}Cl value for the bulk mantle is estimated to be in the range -0.69‰ to -0.37‰ with the mean value of -0.53±0.16‰ from an iterative calculation repeated more than 10000 times (Fig. 11b, 12). Our calculations therefore show that the bulk mantle is slightly depleted in ^{37}Cl with a δ^{37}Cl value of ca. -0.53±0.16‰ relative to SMOC. This agrees well with δ^{37}Cl values measured from terrestrial mantle-derived material and the most pristine type C chondrites, which form a peak between -0.3‰ to -0.1‰ (Sharp et al., 2013; Eggenkamp and Koster van Groos, 1997). Finally, we conclude that the heterogeneous distribution of δ^{37}Cl values represented by this range resulted from metamorphism related to subduction over a range of P-T conditions.

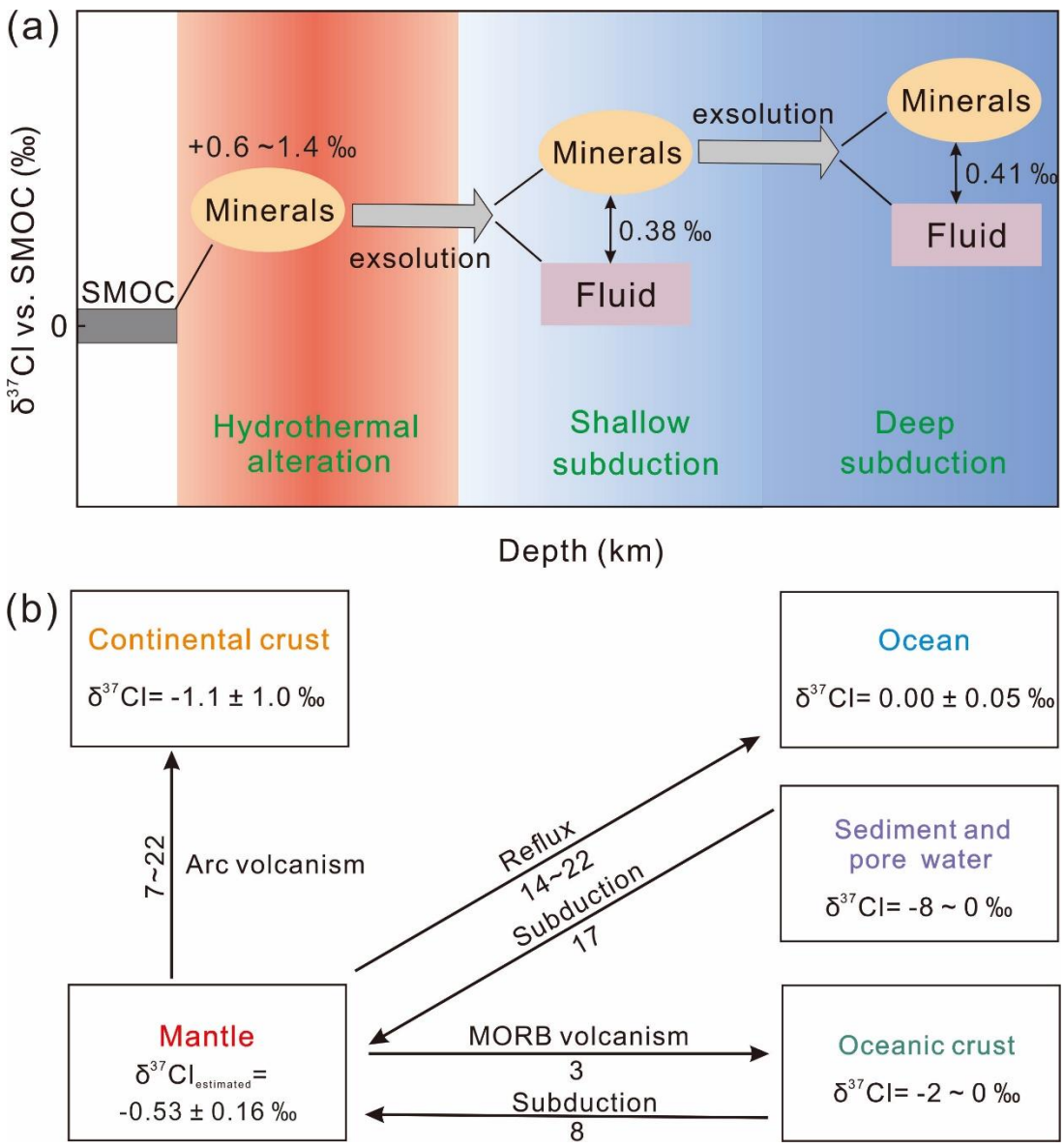

Figure 11. (a) Variation of δ^{37}Cl as a result of processes related to hydrothermal alteration near spreading centers and subduction zones; (b) δ^{37}Cl values of bulk mantle derived from the exchange of chlorine among continental crust, oceanic crust, ocean, sediment. The chlorine fluxes (simplified, 10^{12} g·year^{-1}) are from Eggenkamp (2014) and the δ^{37}Cl values of the individual reservoirs are from Barnes and Sharp (2017).

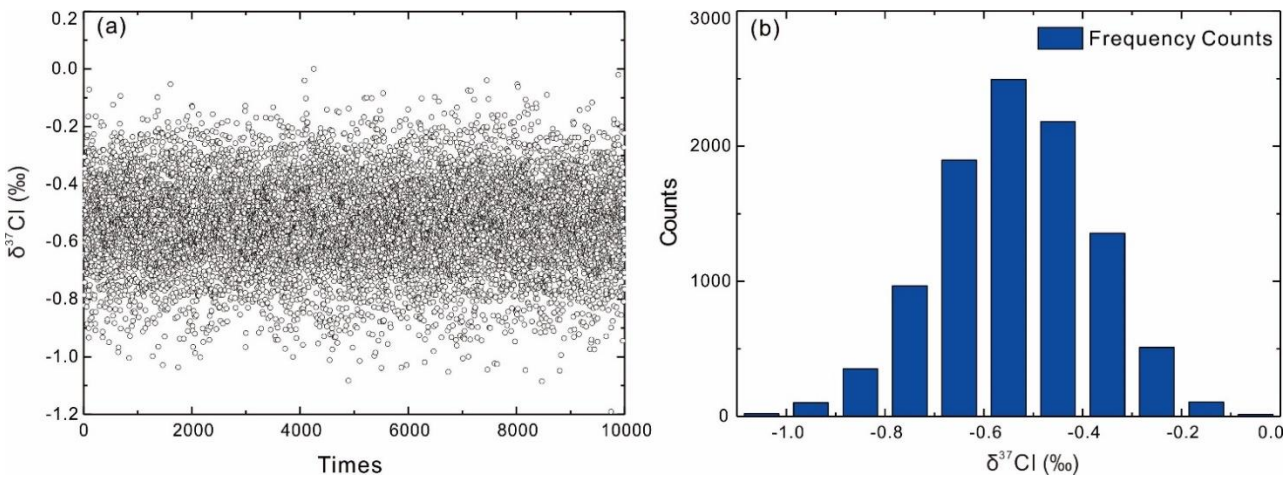

Figure 12. (a) Estimated δ^{37}Cl values of the bulk mantle from an iterative calculation based on mass balance; (b) Frequency distribution δ^{37}Cl values in the bulk mantle.

5. Conclusions

An evaluation of equilibrium chlorine isotope fractionation among chlorine-bearing minerals (apatite-group minerals, muscovite, phlogopite, tremolite, lizardite, marialite, sodium chloride) using first-principles calculations leads to the following conclusions:

(1) At ambient P-T conditions, the ^{37}Cl enrichment in minerals follows the order, phlogopite > muscovite > tremolite > lizardite > fluoro-chlorapatite > hydroxyl-chlorapatite > chlorapatite > sodium chloride > marialite. The 1000lnβ factors are strongly correlated with the metal-Cl bond length and the bond strength of the minerals, such that, in minerals in which chlorine is bonded to trivalent metals (e.g., Al^{3+}), the metal-Cl bonds are shorter and the β factors higher than for minerals, in which the chlorine is bonded to monovalent metals (e.g., Na^{+}) and metal-Cl bonds are long.

(2) Pressure affects the chlorine isotope fractionation for the minerals studied due to the integrated effects of the adjacent atomic environment and the crystal sites of the chlorine atoms, compressibility and the Cl-metal coordination numbers. As a result, the sensitivity to pressure, expressed as 10^3lnβ, follows the order of halite > fluoro-chlorapatite > chlorapatite > marialite > hydroxyl-chlorapatite >

lizardite > tremolite > muscovite > phlogopite.

(3) During the subduction of crustal rocks and sediments, slab fluids released by compaction of sediments or dehydration of altered ocean crust are enriched in chloride and other fluid mobile elements. Assuming that equilibrium is reached, the maximum δ^{37}Cl variation in mantle minerals is estimated to be from -6‰ to +3‰, which compares favorably with the measured range of -1.9‰ to +3‰. By comparison, the estimated δ^{37}Cl value for the bulk mantle relative to SMOC is -0.53‰. Based on our modeling of the contributions of chlorine from multiple reservoirs in the broader context of the global chlorine cycle, we propose that the observed heterogeneous distribution of δ^{37}Cl values in mantle materials is the result of isotope fractionation associated with the interaction of aqueous fluids with minerals during metamorphism related to subduction over a range of P-T conditions.

Declaration of Competing Interest: The authors declare no conflict of interest.

Acknowledgements

The research was supported financially by the National Natural Science Foundation of China (Grants Nos. 41973005, 41673001, 41422302, 41830428). We are grateful to the High Performance Computing Center (HPCC) of Nanjing University for performing the numerical calculations for this paper on its blade cluster system. The authors are grateful to the anonymous reviewers for their constructive and insightful comments that have improved the manuscript significantly. The careful editorial handling by Prof. D. Porcelli is greatly appreciated.

Appendix A. Supplementary data associated with this article can be found, in the online version.

REFERENCES

Agrinier P., Destrigneville C., Giunta T., Bonifacie M., Bardoux G., Andre J. and Lucazeau F. (2019) Strong impact of ion filtration on the isotopic composition of chlorine in young clay-rich oceanic sediment pore fluids. *Geochim. Cosmochim. Acta* **245**, 525-541.

Alexeeva L. P., Alexeev S. V., Kononov A. M., Teng M. and Yunde L. (2015) Halogen isotopes (^{37}Cl and ^{81}Br) in brines of the Siberian Platform. *Procedia Earth & Planetary Science* **13**, 47-51.

Almeida K. M. F. and Jenkins D. M. (2017) Stability field of the Cl-rich scapolite marialite. *Am. Mineral.* **102**, 2484-2493.

Andersson S. S., Wagner T., Jonsson E., Fusswinkel T. and Whitehouse M. J. (2019) Apatite as a tracer of the source, chemistry and evolution of ore-forming fluids: The case of the Olserum-Djupedal REE-phosphate mineralisation, SE Sweden. *Geochim. Cosmochim. Acta* **255**, 163-187.

Anselmi B., Mellini M., and Viti C. (2000) Chlorine in the Elba, Monti Livornesi and Murlo serpentines: evidence for sea-water interaction. *Eur. J. Mineral.* **12**, 137-146.

Antonelli M. A., Schiller M., Schauble E. A., Mittal T., DePaolo D. J., Chacko T., Grew E. S. and Tripoli B. (2019) Kinetic and equilibrium Ca isotope effects in high-T rocks and minerals. *Earth Planet. Sci. Lett.* **517**, 71-82.

Baker J. and Newton R. C. (1994) Standard thermodynamic properties of meionite, $Ca_4Al_6Si_6O_{24}CO_3$, from experimental phase equilibrium data. *Am. Mineral.* **79**, 478-484.

Balan E., Créon L., Sanloup C., Aléon J., Blanchard M., Paulatto L., and Bureau H. (2019) First-principles modeling of chlorine isotope fractionation between chloride-bearing molecules and minerals. *Chem. Geol.* **525**, 424-434.

Bao H., Barnes J. D., Sharp Z. D., and Marchant D. R. (2008) Two chloride sources in soils of the McMurdo Dry Valleys, Antarctica. *J. Geophys. Res. – Atmos.* **113**, 1-10.

Barnes J. D. and Sharp Z. D. (2006) A chlorine isotope study of DSDP/ODP serpentinized ultramafic rocks: Insights into the serpentinization process. *Chem. Geol.* **228**, 246–265.

Barnes J. D., Sharp Z. D. and Fischer T. P. (2008) Chlorine isotope variations across the Izu-Bonin-Mariana arc. *Geology* **36**, 883-886.

Barnes J. D. and Straub S. M. (2010) Chorine stable isotope variations in Izu Bonin tephra: implications for serpentinite subduction. *Chem. Geol.* **272**, 62-74.

Barnes J. D. and Sharp Z. D. (2017) Chlorine isotope geochemistry. *Rev. Mineral. Geochem.* **82**, 345-378.

Bayliss, P., 1987. Mineral nomenclature: scapolite. Mineral. Mag. 51 (359), 176.

Beekman H. E., Eggenkamp H. G. M. and Appelo C. A. J. (2011) An integrated modelling approach to reconstruct complex solute transport mechanisms-Cl and δ^{37}Cl in pore water of sediments from a former brackish lagoon in The Netherlands. *Appl. Geochem.* **26**, 257-268.

Bernal N. F., Gleeson S. A., Dean A. S., Liu X. M. and Hoskin P. (2014) The source of halogens in geothermal fluids from the Taupo Volcanic Zone, North Island, New Zealand. *Geochim. Cosmochim. Acta* **126**, 265-283.

Bernal N. F., Gleeson S. A., Smith M. P., Barnes J. D. and Pan Y. (2017) Evidence of multiple halogen sources in scapolites from iron oxide-copper-gold (IOCG) deposits and regional NaCl metasomatic alteration, Norrbotten County, Sweden. *Chem. Geol.* **451**, 90-103.

Berglund M. and Wieser M. E. (2011) Isotopic compositions of the elements 2009 (IUPAC Technical Report). *Pure Appl. Chem.* **83**, 397-410.

Bigeleisen J. and Mayer M. G. (1947) Calculation of equilibrium constants for isotopic exchange reactions. *J. Chem. Phys.* **15**, 261-267.

Blanchard M., Poitrasson F., Méheut M., Lazzeri M., Mauri F. and Balan E. (2009) Iron isotope fractionation between pyrite (FeS_2), hematite (Fe_2O_3) and siderite ($FeCO_3$): A first-principles density functional theory study. *Geochim. Cosmochim. Acta* **73**, 6565-6578.

Blanchard M., Balan E. and Schauble E. A. (2017) Equilibrium Fractionation of Non-traditional Isotopes: a molecular modeling perspective. *Rev. Mineral. Geochem.* **82**, 27-63.

Bonifacie M., Charlou J. L., Jendrzejewski N., Agrinier P. and Donval J.P. (2005) Chlorine isotopic compositions of high temperature hydrothermal vent fluids over ridge axes. *Chem. Geol.* **221**, 279-288.

Bonifacie M., Jendrzejewski N., Agrinier P., Coleman M., Pineau F. and Javoy M. (2007) Pyrohydrolysis-IRMS determination of silicate chlorine stable isotope compositions. Application to oceanic crust and meteorite samples. *Chem. Geol.* **242(1-2)**, 187-201.

Bonifacie M., Busigny V., Mével C., Philippot P., Agrinier P., Jendrzejewski N., Scambelluri M. and Javoy M. (2008) Chlorine isotopic composition in seafloor serpentinites and high-pressure metaperidotites. Insights into oceanic serpentinization and subduction processes. *Geochim. Cosmochim. Acta* **72**, 126-139.

Capitani G. C. and Stixrude L. (2012) A first-principle investigation of antigorite up to 30 GPa: Structural behavior under compression. *Am. Mineral.* **97**, 1177-1186.

Chiaradia M., Barnes J. D. and Cadet-Voisin S. (2014) Chlorine stable isotope variations across the Quaternary volcanic arc of Ecuador. *Earth Planet. Sci. Lett.* **396**, 22-33.

Clark S. J., Segall M. D., Pickard C.J., Hasnip P. J., Probert M. I. J., Refson K. and Payne M. C. (2005) First principles methods using CASTEP. *Z. Krist-Cryst. Mater.* **220**, 567-570.

Comodi P., Mellini M., Ungaretti L. and Zanazzi P. F. (1991) Compressibility and High-Pressure Structure Refinement of Tremolite, Pargasite and Glaucophane. *Eur. J. Mineral.* **3**, 485-499.

Comodi P., Liu Y., Zanazzi P. F. and Montagnoli M. (2001) Structural and vibrational behaviour of fluorapatite with pressure. Part I: in situ single-crystal X-ray diffraction investigation. *Phys. Chem. Miner.* **28**, 219-224.

Cullen J. T., Barnes J. D., Hurwitz S. and Leeman W. P. (2015) Tracing chlorine sources of thermal and mineral springs along and across the Cascade Range using halogen concentrations and chlorine isotope compositions. *Earth Planet. Sci. Lett.* **426**, 225-234.

Czarnacki M., and Halas S. (2012) Isotope fractionation in aqua-gas systems: Cl_2-HCl-Cl^-, Br_2-HBr-Br^- and H_2S-S^{2-}. *Isotopes Environ. Health Stud.* **48**, 55-64.

Dódony I. and Buseck P. R. (2004) Serpentine close-up and intimate: An HRTEM view. *Int. Geol. Rev.* **46**, 507-527.

Dove M. T. (1993) *Introduction to Lattice Dynamics.* Cambridge University Press, Cambridg.

Downs R. T., Hall-Wallace M. (2003). The *American Mineralogist* crystal structure database. *Am. Mineral.* **88**, 247-250.

Eastoe C. J., Guilbert J. M. and Kaufmann R. S. (1989) Preliminary evidence for fractionation of stable chlorine isotopes in ore forming hydrothermal systems. *Geology* **17**, 285-288.

Eastoe C. J. and Guilbert J. M. (1992) Stable chlorine isotopes in hydrothermal processes. *Geochim. Cosmochim. Acta* **56**, 4247-4255.

Eastoe C. J., Long A.and Knauth L. P. (1999) Stable chlorine isotopes in the Palo Duro Basin, Texas: evidence for preservation of Permian evaporite brines. *Geochim. Cosmochim. Acta* **63**, 1375-1382.

Eastoe C. J., Long A., Land L. S.and Kyle J. R. (2001) Stable chlorine isotopes in halite and brine from the Gulf Coast Basin: brine genesis and evolution. *Chem. Geol.* **176**, 343-360.

Eastoe C. J. (2016) Stable chlorine isotopes in arid non-marine basins: Instances and possible fractionation mechanisms. *Appl. Geochem.* **74**, 1-12.

Eggenkamp H. G. M., Middelburg J. J. and Kreulen R. (1994) Preferential diffusion of ^{35}C1 relative to ^{37}C1 in sediments of Kau Bay, Halmahera, Indonesia. *Chem. Geol.* **116**, 317-325.

Eggenkamp H. G. M., Kreulen R. and Koster van Groos A. F. (1995) Chlorine stable isotope fractionation in evaporites. *Geochim. Cosmochim. Acta* **59**, 5169-5175.

Eggenkamp H. G. M. and Koster van Groos A. F. (1997) Chlorine stable isotopes in carbonatites: Evidence for isotopic heterogeneity in the mantle. *Chem. Geol.* **140**, 137-143.

Eggenkamp H. G. M. and Coleman M. L. (2009) The effect of aqueous diffusion on the fractionation of chlorine and bromine stable isotopes. *Geochim. Cosmochim. Acta* **73**, 3539-3548.

Eggenkamp H. G. M. (2014) The geochemistry of stable chlorine and bromine isotopes. In *Advances in Isotope Geochemistry* (ed. J. Hoefs). Springer-Verlag, Heidelberg.

Eggenkamp H. G. M., Bonifacie M., Ader M. and Agrinier P. (2016) Experimental determination of stable chlorine and bromine isotope fractionation during precipitation of salt from a saturated solution. *Chem. Geol.* **433**, 46-56.

Eggenkamp H. G. M., Louvat P., Agrinier P., Bonifacie M., Bekker A., Krupenik V., Griffioen J., Horita J., Brocks J.J. and Bagheri R. (2019a) The bromine and chlorine isotope composition of primary halite deposits and their significance for the secular isotope composition of seawater. *Geochim. Cosmochim. Acta* **264**, 13-29.

Eggenkamp H. G. M., Louvat P., Griffioen J. and Agrinier P. (2019b) Chlorine and bromine isotope evolution within a fully developed Upper Permian natural salt sequence. *Geochim. Cosmochim. Acta* **245**, 316-326.

Eggenkamp H. G. M., Marks M. A.W., Atanasova P., Wenzel T., and Mark G. (2020) Changes in halogen (F, Cl, Br, and I) and S ratios in rock-forming minerals as monitors for magmatic differentiation, volatile-loss, and hydrothermal overprint: The case for peralkaline systems. *Minerals* **10**, 995.

Feng C., Qin T., Huang S., Wu Z., and Huang F. (2014). First-principles investigations of equilibrium calcium isotope fractionation between clinopyroxene and Ca-doped orthopyroxene. *Geochim. Cosmochim. Acta* **143**, 132-142.

Gleeson S. A. and Smith M. P. (2009) The sources and evolution of mineralising fluids in iron oxide-copper-gold systems, Norrbotten, Sweden: Constraints from Br/Cl ratios and stable Cl isotopes of fluid inclusion leachates. *Geochim. Cosmochim. Acta* **73**, 5658-5672.

Godon A., Jendrzejewski N., Eggenkamp H. G. M., Banks D. A., Ader M., Coleman M. L. and Pineau F. (2004) A cross-calibration of chlorine isotopic measurements and suitability of seawater as the international reference material. *Chem. Geol.* **207(1-2)**, 1-12.

Green D. H. and Wallace M. E. (1988) Mantle metasomatism by ephemeral carbonatite melts. *Nature* **336**, 459.

Gregory R. T. and Taylor H. P. Jr. (1981) An oxygen isotope profile in a section of Cretaceous oceanic crust, Samail Ophiolite, Oman: evidence for ^{18}O buffering of the oceans by deep (>5 km) seawater-hydrothermal circulation at mid-ocean ridges. *J. Geophys. Res. Solid Earth* **86**, 2737-2755.

Hanley J., Ames D., Barnes J., Sharp Z. and Guillong M. (2011) Interaction of magmatic fluids and silicate melt residues with saline groundwater in the footwall of the Sudbury Igneous Complex, Ontario, Canada: New evidence from bulk rock geochemistry, fluid inclusions and stable isotopes. *Chem. Geol.* **281**, 1-25.

Hay W. W., Migdisov A., Balukhovsky A. N., Wold C. N., Flögel S., and Söding E. (2006) Evaporites and the salinity of the ocean during the Phanerozoic: Implications for climate, ocean circulation and life. *Palaeogeogr. Palaeocl.* **240**, 3-46.

Hilairet N., Daniel I., and Reynard B. (2006) P-V Equations of State and the relative stabilities of serpentine varieties. *Phys. Chem. Miner.* **33**, 629-637.

Horita J., Cole D. R., Polyakov V. B. and Driesner T. (2002) Experimental and theoretical study of pressure effects on hydrogen isotope fractionation in the system brucite-water at elevated temperatures. *Geochim. Cosmochim. Acta* **66**, 3769-3788.

Huang F., Chen L., Wu Z. and Wang W. (2013) First-principles calculations of equilibrium Mg isotope fractionations between garnet, clinopyroxene, orthopyroxene, and olivine: Implications for Mg isotope thermometry. *Earth Planet. Sci. Lett.* **367**, 61-70.

Huang F., Wu Z., Huang S. and Wu F. (2014) First-principles calculations of equilibrium silicon isotope fractionation among mantle minerals. *Geochim. Cosmochim. Acta* **140**, 509-520.

Huang F., Zhou C., Wang W., Kang J. and Wu Z. (2019) First-principles calculations of equilibrium Ca isotope fractionation: Implications for oldhamite formation and evolution of lunar magma ocean. *Earth Planet. Sci. Lett.* **510**, 153-160.

Hughes J. M. and Rakovan J. (2015) Structure and chemistry of apatite and apatite supergroup minerals. *Elements* **11**, 165-170.

John T., Layne G. D., Haase K. M. and Barnes J.D. (2010) Chlorine isotope evidence for crustal recycling into the Earth's mantle. *Earth Planet. Sci. Lett.* **298(1-2)**, 175-182.

Kamenetsky V. S., Mitchell R. H., Maas R., Giuliani A., Gaboury D. and Zhitova L. (2015) Chlorine in mantle-derived carbonatite melts revealed by halite in the St.- Honoré intrusion (Quebec, Canada) *Geology* **43(8)**, 687-690.

Kaufmann R., Long A., Bentley H. and Davis S. (1984) Natural chlorine isotope variations. *Nature* **309(5966)**, 338-340.

Kieffer and Werner S. (1982) Thermodynamics and lattice vibrations of minerals: 5. Applications to phase equilibria, isotopic fractionation, and high-pressure thermodynamic properties. *Rev. Geophys.* **20**, 827-849.

Kirby S. H. (1987) Localized polymorphic phase transformations in high-pressure faults and applications to the physical mechanism of deep earthquakes. *J. Geophys. Res. B, Solid Earth* **92**, 13789-13800.

Konzett J. and Frost D. J. (2009) The high P-T stability of hydroxyl-apatite in natural and simplified MORB-an experimental study to 15 GPa with implications for transport and storage of phosphorus and halogens in subduction zones. *J. Petro*. **50(11)**, 2043-2062.

Kowalski P. M. and Jahn S. (2011) Prediction of equilibrium Li isotope fractionation between minerals and aqueous solutions at high P and T: an efficient ab initio approach. *Geochim. Cosmochim. Acta* **75(20)**, 6112-6123.

Kowalski P. M., Wunder B. and Jahn S. (2013) *Ab initio* prediction of equilibrium boron isotope fractionation between minerals and aqueous fluids at high P and T. *Geochim. Cosmochim. Acta* **101**, 285-301.

Kullerud, K. and Erambert M. (1999) Cl-scapolite, Cl-amphibole, and plagioclase equilibria in ductile shear zones at Nusfjord, Lofoten, Norway: Implications for fluid compositional evolution during fluid-mineral interaction in the deep crust. *Geochim. Cosmochim. Acta* **63**, 3829-3844.

Li L., Bonifacie M., Aubaud C., Crispi O., Dessert C. and Agrinier P. (2015) Chlorine isotopes of thermal springs in arc volcanoes for tracing shallow magmatic activity. *Earth Planet. Sci. Lett.* **413**, 101-110.

Li W., Kwon K. D., Li S., and Beard B. L. (2017) Potassium isotope fractionation between K-salts and saturated aqueous solutions at room temperature: Laboratory experiments and theoretical calculations. *Geochim. Cosmochim. Acta* **214**, 1-13.

Liebscher A., Barnes J. and Sharp Z. D. (2006) Chlorine isotope vapor–liquid fractionation during experimental fluid-phase separation at 400 °C/23 MPa to 450°C/42 MPa. *Chem. Geol.* **234**, 340-345.

Liu Y. and Tossell J.A. (2005) *Ab initio* molecular orbital calculations for boron isotope fractionations on boric acids and borates. *Geochim. Cosmochim. Acta* **69**, 3995-4006.

Lotti P., Comboni D., Merlini M. and Hanfland M. (2018) High-pressure behavior of intermediate scapolite: compressibility, structure deformation and phase transition. *Phys. Chem. Miner*. **45**, 945-962.

Luth R. W. (2014) Volatiles in Earth's Mantle. In T*reatise of Geochemistry 2nd Edition* (ed. H. D. Holland and K. K. Turekian). Elsevier-Pergamon, Oxford, pp. 377-378.

Marques J. M., Eggenkamp H. G. M., Carreira P. M., and Antunes da Silva M. (2020) Origin and evolution of Cl in CO_2-rich thermal and mineral waters from northern Portugal. *Appl. Geochem.* **116**, 104569.

McDonough W.F. (2000) The composition of the earth. In: Teisseyre R., Majewski E. (Eds.), Earthquake thermodynamics and phase transformations in the earth's interior.

Meade C. and Jeanloz R. (1990) The strength of mantle silicates at high pressures and room temperature: implications for the viscosity of the mantle. *Nature* **348**, 533-535.

Meade C. and Jeanloz R. (1991) Deep-focus earthquakes and recycling of water into the Earth's mantle. *Science* **252**, 68-72.

Méheut M., Lazzeri M., Balan E. and Mauri F. (2007) Equilibrium isotopic fractionation in the kaolinite, quartz, water system: Prediction from first-principles density-functional theory. *Geochim. Cosmochim. Acta* **71**, 3170-3181.

Méheut M., Lazzeri M., Balan E. and Mauri F. (2009) Structural control over equilibrium silicon and oxygen isotopic fractionation: A first-principles density-functional theory study. *Chem. Geol.* **258**, 28-37.

Méheut M. and Schauble E. A. (2014) Silicon isotope fractionation in silicate minerals: Insights from first-principles models of phyllosilicates, albite and pyrope. *Geochim. Cosmochim. Acta* **134**, 137-154.

Mellini M. and Zanazzi P. F. (1989) Effects of pressure on the structure of lizardite-1T. *Eur. J. Mineral.* **1**, 13-19.

Mellini M.and Viti C. (1994) Crystal structure of lizardite-1T from Elba, Italy. *Am. Mineral.* **79(11)**, 1194-1198.

Murayama, J. K., Nakai, S., Kato, M. and Kumazawa, M. (1986) A dense polymorph of $Ca_3(PO_4)_2$: a high pressure phase of apatite decomposition and its geochemical significance. *Phys. Earth Planet. In.* **44**, 293-303.

Nahnybida T., Gleeson S. A., Rusk B., and Wassenaar L. I. (2009). Cl/Br ratios and stable chlorine isotope analysis of magmatic–hydrothermal fluid inclusions from Butte, Montana and Bingham Canyon, Utah. *Miner. Depos.* **44**(8), 837-848.

Pan Y. and Fleet M. E. (2002) Compositions of the apatite-group minerals: substitution mechanisms and controlling factors. *Rev. Mineral. Geochem.* **48**, 13-49.

Palme H. and O'Neill H. (2014) Cosmochemical estimates of mantle composition. In *Treatise on Geochemistry 2nd Edition* (ed. M. D. Andrew). Elsevier, Oxford.

Perdew J. P., Burke K., and Ernzerhof M. (1996) Generalized gradient approximation made simple. *Phys. Rev. Lett.* **77**, 3685-3868.

Petrini K., Podladchikov Y. (2000) Lithospheric pressure-depth relationship in compressive region of thickened crust. *J. Metamorphic Geol.* **18**, 67-77.

Piccoli, P.M., Candela, P.A., 2002. Apatite in Igneous Systems. Rev. Mineral. Geochem. 48 (1), 255–292.

Polyakov V.B. and Kharlashina N.N. (1994) Effect of Pressure on Equilibrium Isotopic Fractionation. *Geochim. Cosmochim. Acta* **58**, 4739-4750.

Richard A., Banks D. A., Mercadier J., Boiron M. C., Cuney M. and Cathelineau M. (2011) An evaporated seawater origin for the ore-forming brines in unconformityrelated uranium deposits (Athabasce Basin, Canada): Cl/Br and δ^{37}Cl analysis of fluid inclusions. *Geochim. Cosmochim Acta* **75**, 2792-2810.

Ringwood A.E. (1975) Composition and petrology of the earth's mantle. McGraw-Hill, New York. 618 p.

Rizzo A. L., Caracausi A., Liotta M., Paonita A., Barnes J. D., Corsaro R. A. and Martelli M. (2013) Chlorine isotopic composition of volcanic gases and rocks at Mount Etna (Italy) and inferences on the local mantle source. *Earth Planet. Sci. Lett.* **371**, 134-142.

Rudnick R. L. and Gao S. (2003) Composition of the Continental Crust. In *Treatise on geochemistry* (ed. R. L. Rudnick). Elsevier, Oxford.

Rustad J. R., Bylaska E. J., Jackson V. E., and Dixon D.A. (2010) Calculation of boron-isotope fractionation between $B(OH)_3$ (aq) and $B(OH)_4^-$ (aq). *Geochim. Cosmochim Acta* **74**(10), 2843-2850.

Schauble E. A., Rossman G. R. and Taylor H. P. (2003) Theoretical estimates of equilibrium chlorine-isotope fractionations. *Geochim. Cosmochim. Acta* **67**, 3267-3281.

Schauble E. A. (2004) Applying stable isotope fractionation theory to new systems. *Rev. Mineral. Geochem.* **55**, 65-111.

Schauble E. A., Ghosh P. and Eiler J. M. (2006) Preferential formation of ^{13}C-^{18}O bonds in carbonate minerals, estimated using first-principle lattice dynamics. *Geochim. Cosmochim. Acta* **70(10)**, 2510-2529.

Schauble E. A., Meheut M. and Hill P. S. (2009) Combining Metal Stable Isotope Fractionation Theory with Experiments. *Elements* **5**, 369-374.

Schauble E. A. (2011) First-principles estimates of equilibrium magnesium isotope fractionation in silicate, oxide, carbonate and hexaaquamagnesium(2+) crystals. *Geochim. Cosmochim. Acta* **75**, 844-869.

Schmidt M. W., Dardon A., Chazot G., and Vannucci R. (2004) The dependence of Nb and Ta rutile-melt partitioning on melt composition and Nb/Ta fractionation during subduction processes. *Earth Planet. Sci. Lett.* **226**, 415-432.

Sharp Z. D., Barnes J. D., Brearley A. J., Chaussidon M., Fischer T.P. and Kamenetsky V.S. (2007) Chlorine isotope homogeneity of the mantle, crust and carbonaceous chondrites. *Nature* **446,** 1062-1065.

Sharp Z. D., Shearer C. K., McKeegan K. D., Barnes J. D. and Wang Y. Q. (2010) The chlorine isotope composition of the moon and implications for an anhydrous mantle. *Science* **329(5995)**, 1050-1053.

Sharp Z. D., Mercer J. A., Jones R. H., Brearley A. J., Selverstone J., Bekker. A., Stachel T. (2013) The chlorine isotope composition of chondrites and Earth. *Geochim. Cosmochim. Acta* **107**, 189-204.

Shouakar-Stash O., Frape S. K., Drimmie R. J. (2003). Stable hydrogen, carbon and chlorine isotope measurements of selected chlorinated organic solvents. *J. Contam. Hydrol.* **60**, 211-228.

Shouakar-Stash O., Drimmie R. J., Zhang M., and Frape S. K. (2006) Compound-specific chlorine isotope ratios of TCE, PCE and DCE isomers by direct injection using CF-IRMS. *Appl. Geochem.* ***21(5)***, 766-781.

Shouakar-Stash O., Alexeev S. V., Frape S. K., Alexeeva L. P., Drimmie R. J. (2007). Geochemistry and stable isotopic signatures, including chlorine and bromine isotopes, of the deep groundwaters of the Siberian Platform, Russia. *Appl. Geochem.* **22**, 589-605.

Skippen G. B. (1971) Experimental data for reactions in siliceous marbles. *J. Geol.* **79(4)**, 457-481.

Stewart M. A., Klein E. M., Spivack A. J. and Schilling J. G. (1998) Stable chlorine isotope compositions of N- and E-MOR basalt glasses from the north Atlantic. Eos Trans. *Am. Geophys. Union* 79, 954 (abstract).

Stewart M. A. and Spivack A.J. (2004) The stable-chlorine isotope compositions of natural and anthropogenic materials. *Rev. Mineral. Geochem.* **55(1)**, 231-254.

Stotler R. L., Frape S. K. and Shouakar-Stash O. (2010) An isotopic survey of δ^{81}Br and δ^{37}Cl of dissolved halides in the Canadian and Fennoscandian shields. *Chem. Geol.* **274**, 38-55.

Tsuchiya J. (2013) A first-principles calculation of the elastic and vibrational anomalies of lizardite under pressure. *Am. Mineral.* **98**, 2046-2052.

Volpe C. and Spivack A. J. (1994) Stable chlorine isotopic composition of marine aerosol particles in the western atlantic ocean. *Geophys. Res. Lett.* **21(12)**, 1161-1164.

Wang W., Qin T., Zhou C., Huang S., Wu Z., and Huang, F. (2017). Concentration effect on equilibrium fractionation of Mg-Ca isotopes in carbonate minerals: Insights from first-principles calculations. *Geochim. Cosmochim. Acta* **208**, 185-197.

Wang W., Zhou C., Liu Y., Wu Z., Huang F. (2019). Equilibrium mg isotope fractionation among aqueous mg2+, carbonates, brucite and lizardite: insights from first-principles molecular dynamics simulations. *Geochim. Cosmochim. Acta* **250**, 117-129.

Wang X., Hu W. and Chou I-M. (2013) Raman spectroscopic characterization on the OH stretching bands in NaCl–Na_2CO_3–Na_2SO_4–CO_2–H_2O systems: Implications for the measurement of chloride concentrations in fluid inclusions. *J. Geochem. Explor.* **132**, 111-119.

Wicks F. J. and O'Hanley D. (1988) Serpentine minerals: structure and petrology. In *Reviews in Mineralogy: Hydrous phyllosilicates* (ed. S. W. Bailey). Mineralogical Society of America, Washington DC, pp 91–167.

Williams, Q., Knittle, E., Scott, H.P., Liu, Z., 2012. The high-pressure behavior of micas: Vibrational spectra of muscovite, biotite, and phlogopite to 30 GPa. Am. Mineral. 97 (1), 241–252.

Willmore C. C., Boudreau A. E., Spivack A. and Kruger F. J. (2002) Halogens of bushveld complex, south Africa: δ^{37}Cl and Cl/F evidence for hydration melting of the source region in a back-arc setting. *Chem. Geol.***182**, 503-511.

Wu Z., Huang F. and Huang S. (2015) Isotope fractionation induced by phase transformation: First-principles investigation for Mg_2SiO_4. *Earth Planet. Sci. Lett.* **409**, 339-347.

Young E. D., Manning C. E., Schauble E. A., Shahar A., Macris C. A., Lazar C. and Jordan M. (2015) High-temperature equilibrium isotope fractionation of non-traditional stable isotopes: experiments, theory, and applications. *Chem. Geol.* **395**, 176-195.

Zhao Y., Wei H. Z., Liu X., Wang Y. J., Jiang S. Y., Eastoe C. J., Peryt T. M. (2021) Isotope evidence for multiple sources of B and Cl in Middle Miocene (Badenian) evaporites, Carpathian Mountains. *Appl. Geochem.* **124**, 104819

Zhang W. W., Oganov A. R., Goncharov A. F., Zhu Q., Boulfelfel S. E., Lyakhov A. O., Stavrou E., Somayazulu M., Prakapenka V. B. and Konopkova Z. (2013) Unexpected Stable Stoichiometries of Sodium Chlorides. *Science* **342**, 1502-1505.

Zheng Y. F. (1993a) Calculation of oxygen isotope fractionation in hydroxyl-bearing silicates. *Earth Planet. Sci. Lett.* **120**, 247-263.

Zheng Y. F. (1993b) Calculation of oxygen isotope fractionation in anhydrous silicate minerals. *Geochim. Cosmochim. Acta* **57**, 1079-1091.

Zheng Y. F. (1995) Oxygen isotope fractionation in magnetites: structural effect and oxygen inheritance. *Chem. Geol.* **121**, 309-316.

Zheng Y. F. (1996) Oxygen isotope fractionations involving apatites: Application to paleotemperature determination. *Chem. Geol.* **127(1-3)**, 177-187.

Zheng Y. F. (1998) Oxygen isotope fractionation between hydroxide minerals and water. *Phys. Chem. Miner.* **25**, 213-221.

Zheng Y. F., Wei C. S., Zhou G. T., Xu B. L. (1998) Oxygen isotope fractionation in mantle minerals. *Sci. China Ser. D: Earth Sciences* **41**, 95-103.

Zheng Y. F. (1999) Oxygen isotope fractionation in carbonate and sulfate minerals. *Geochem. J.* **33**, 109-126.

Zheng Y. F. (2009) Fluid regime in continental subduction zones: Petrological insights from ultrahigh-pressure metamorphic rocks. *J Geol Soc.* **166**, 763-782.

Zheng Y. F, Hermann J. (2014) Geochemistry of continental subduction- zone fluids. *Earth Planets Space* **66**, 93.

Zheng Y. F. and Böttcher M. E. (2016) Oxygen isotope fractionation in double carbonates. *Isotopes Environ. Health Stud.* **52(1-2)**, 29-46.

Zheng Y. F. and Chen R. X. (2017) Regional metamorphism at extreme conditions: Implications for orogeny at convergent plate margins. *J. Asian Earth Sci.* **145**, 46-73.

CAPTIONS OF FIGURES AND TABLE

Figure 1. Chlorine isotope variability in mantle-derived materials (Bonifacie et al. 2007, 2008; Sharp et al., 2007; John et al., 2010). EPR: East Pacific Rise; PAR: Pacific Antarctic Ridge; CRR: Costa Rica Rift; SH: St. Helena; M.: McDonald; E.: Easter; F.: Foundation; P.: Pitcairn; S.: Societies; R.: Réunion.

Figure 2. A series of periodic boundary cell (PBC) models for minerals, presented as top and side views.

Figure 3. Comparison of calculated and experimentally determined vibrational frequencies for chlorine-bearing minerals. The measured vibrational frequencies are from previous studies, as listed in Table S3 in the Appendix.

Figure 4. Temperature dependence of the equilibrium reduced partition function ratios $10^3\ln\beta$ for chlorine isotopes in chlorine-bearing minerals at 0 GPa. The data for halite[1] are from Schauble et al. (2003). The data for Cl-Ap[1], halite[2] and lizardite[1] are from Balan et al. (2019).

Figure 5. Equilibrium reduced partition function ratios $10^3\ln\beta$ as a function of the metal-Cl bond length (a) and the metal-Cl bond strength (b) in chlorine-bearing minerals at ambient P-T conditions

Figure 6. The dependence of $10^3\ln\beta$ of apatite group minerals on Cl/(OH+Cl) at various temperatures. The insert shows the average Ca-Cl bond length versus Cl/(OH+Cl) at ambient P-T conditions.

Figure 7. Variations in the average metal-Cl bond length for chlorine-bearing minerals with increasing pressure at static condition.

Figure 8. The dependence of the reduced partition function ratios, $10^3\ln(\beta_p/\beta_0)$, on pressure for the $^{37}Cl/^{35}Cl$ ratio of chlorine-bearing minerals (apatite, muscovite, phlogopite, tremolite, lizardite, marialite, halite) as a function of pressure. The term β_0 represents the calculated reduced partition function at 0 GPa.

Figure 9. (a) Temperature dependence of $10^3\ln\beta_A$-$10^3\ln\beta_B$ for $^{37}Cl/^{35}Cl$ between different chlorine-bearing minerals (A) and halite (B) at 0 and 2.5 GPa. The solid lines are for 0 GPa and the dotted lines for 2.5 GPa. (b) Temperature dependence of $10^3\ln\beta_A$-$10^3\ln\beta_B$ for $^{37}Cl/^{35}Cl$ between different chlorine-bearing minerals (A) and aqueous chloride (B) at ambient pressure.

Figure 10. The $\delta^{37}Cl$ values of hydrous minerals in different metamorphic facies including those of subduction-zones. The dark-grey area corresponds to UHP metamorphism above the coesite/quartz transition boundary, whereas the light-grey area denotes HP metamorphism below the coesite/quartz transition line (modified after Zheng and Chen, 2017).

Figure 11. (a) Variation of $\delta^{37}Cl$ as a result of processes related to hydrothermal alteration near spreading centers and subduction zones; (b) $\delta^{37}Cl$ values of bulk mantle derived from the exchange of chlorine among continental crust, oceanic crust, ocean, sediment. The chlorine fluxes (simplified, 10^{12}

g·year^{-1}) are from Eggenkamp (2014) and the δ^{37}Cl values of the individual reservoirs are from Barnes and Sharp (2017).

Figure 12. (a) Estimated δ^{37}Cl values of the bulk mantle from an iterative calculation based on mass balance; (b) Frequency distribution δ^{37}Cl values in the bulk mantle.

Table 1. Calculation sets for chlorine-bearing minerals.